DEPARTMENT OF DEFENCE
DEFENCE SCIENCE & TECHNOLOGY ORGANISATION
DSTO

A Correlation between Flight-determined Longitudinal and Lateral Derivatives and Wind Tunnel Data for the Pilatus PC 9/A Training Aircraft in Approach and Departure Configurations

Nick van Bronswijk,
Andrew D. Snowden,
Hilary A. Keating and
Geoff J. Brian

DSTO-TR-0479

A Correlation between Flight-determined Longitudinal and Lateral Derivatives and Wind Tunnel Data for the Pilatus PC 9/A Training Aircraft in Approach and Departure Configurations

Nick van Bronswijk, Andrew D. Snowden, Hilary A. Keating and Geoff J. Brian

Air Operations Division
Aeronautical and Maritime Research Laboratory

DSTO–TR–0479

ABSTRACT

A series of flight tests were conducted on the PC 9/A aircraft, A23-045, at the Royal Australian Air Force's Aircraft Research and Development Unit. System identification techniques were applied to the data obtained from these flight tests to determine the stability and control derivatives of the aircraft. The longitudinal and lateral results for the aircraft in approach and departure configurations are presented in this report and comparisons are made with wind tunnel estimates.

Published by

DSTO Aeronautical and Maritime Research Laboratory
506 Lorimer St,
Fishermans Bend, Victoria, Australia 3207

Telephone: *(03) 9626 7000*
Facsimile: *(03) 9626 7999*

AR No. AR-011-629
November, 2000

APPROVED FOR PUBLIC RELEASE

A Correlation between Flight-determined Longitudinal and Lateral Derivatives and Wind Tunnel Data for the Pilatus PC 9/A Training Aircraft in Approach and Departure Configurations

EXECUTIVE SUMMARY

Air Operations Division (AOD) has developed, or acquired, a number of fixed-wing flight dynamic models and is also responsible for providing advice to the Australian Defence Organisation (ADO) on flight simulator flight dynamic model requirements. The models generally make use of extensive static and dynamic stability and control derivative databases, in addition to engine and flight control models. The static model data may be obtained from wind tunnel testing, whilst the dynamic data is traditionally obtained from flight tests using system identification techniques.

The system identification techniques used to estimate aerodynamic derivatives of conventional aircraft are well established. The major requirement of these techniques is high fidelity measurements of manoeuvre input (i.e. control surface deflections), and aircraft response (i.e. angular rates and linear accelerations), as well as air data including airspeed, altitude, angle-of-attack and angle-of-sideslip.

Following the completion of the AOD PC 9/A wind tunnel tests, the requirement existed for a dedicated flight dynamic modelling flight test program to both validate the flight dynamic model of the PC 9/A and to provide dynamic derivative estimates that were not obtainable in the AMRL wind tunnel. An instrumentation suite, including an air data probe for the direct and accurate measurement of angle-of-attack, angle-of-sideslip, temperature, and static and dynamic pressure, was fitted to the aircraft and a test manoeuvre matrix was designed specifically for the purpose of gathering flight dynamic data. This flight test program was conducted at the Aircraft Research and Development Unit (ARDU) during 1998/99.

This report details the analysis of the longitudinal and lateral manoeuvres carried out with the aircraft in the approach and departure configurations. The static and dynamic derivatives thus obtained are compared with wind tunnel estimates. A discussion of some of the difficulties encountered during the estimation process is also included. The data obtained from these tests will be used in the development of the PC 9/A flight dynamic model, further enhancing AOD support for the PC 9/A fleet, including possible upgrades to the part-task trainer.

Authors

Nick van Bronswijk
Air Operations Division

Nick van Bronswijk graduated from the University of Sydney with first class honours in Aeronautical Engineering in 1995. He is currently completing his PhD in the area of propeller power effects. Since joining AMRL in 1998 he has been involved with a range of projects including flight and wind tunnel test programs of the Pilatus PC 9/A.

Andrew Snowden
Air Operations Division

Andrew Snowden graduated from the Royal Melbourne Institute of Technology in 1991, having obtained a Bachelor of Engineering in Aerospace Engineering with first class honours. Before commencing work at AMRL he served a short term attachment with McDonnell Douglas in St. Louis, Missouri, as the recipient of the McDonnell Aircraft Company Aerospace Engineering Prize for 1991. He commenced employment at AMRL in 1992 and participated in several experimental investigations in a number of different fields during his rotation. Now a full time member of the flight dynamics and performance area of the Air Operations Division, his most recent work includes the organisation of flight testing for parameter identification of the Pilatus PC 9/A as well as performance estimation of modern jet fighters.

Hilary Keating
Air Operations Division

Hilary Keating graduated from the University of Sydney in 1998, having obtained a Bachelor of Engineering in Aeronautical Engineering with first class honours. She commenced employment at AMRL in 1999, and has been involved in performance modelling and parameter identification of the Pilatus PC 9/A.

Geoff Brian
Air Operations Division

Geoff Brian commenced employment at the Aeronautical and Maritime Research Laboratory in 1989, after graduating from the University of New South Wales with a degree in Aeronautical Engineering, Honours Class 1. During his employment with AMRL, he has been involved with the analysis of flight data for the development of a comprehensive flight dynamic model of the F-111C aircraft; the development of aircraft performance estimation applications; and involvement with a performance flight trial of a F-111C aircraft fitted with Pratt & Whitney TF30-P-109 engines. Mr. Brian was attached to the Royal Australian Air Force – Aircraft Research and Development Unit in 1992, where he was involved with a performance flight trial of an air-to-air refuelling capable Boeing 707 aircraft. During 1998 and 1999 Mr. Brian attended Loughborough University in the United Kingdom being awarded with a MSc in Industrial Mathematical Modelling with Distinction. Mr Brian is currently the manager for aircraft flight dynamic activities at AMRL.

Contents

Appendices

Figures

Tables

Glossary

AHRS	Artificial Horizon Reference System
AMRL	Aeronautical and Maritime Research Laboratory
AOD	Air Operations Division
ARDU	Aircraft Research and Development Unit
DSTO	Defence Science and Technology Organisation
GDAS	General Data Acquisition System
IAS	Indicated Airspeed
ITT	Inlet Turbine Temperature
KIAS	Knots Indicated Airspeed
MAC	Mean Aerodynamic Chord
NASA	National Aeronautics and Space Administration
NG	Gas generator speed
OAT	Outside Air Temperature
PAP	Primary Analysis Processor
RAAF	Royal Australian Air Force
SHP	Shaft Horse Power

Notation

a_X, a_Y, a_Z	Body axes linear accelerations (g)
b	Reference span (10.124 m)
C_l	Rolling moment coefficient $C_l = \frac{l}{\bar{q}Sb}$
C_{l_β}	Rolling moment coefficient due to angle-of-sideslip $C_{l_\beta} = \frac{\partial C_l}{\partial \beta}$ (per degree)
C_{l_p}	Rolling moment coefficient due to roll rate $C_{l_p} = \frac{\partial C_l}{\partial \left(\frac{pb}{2V}\right)}$ (per radian)
C_{l_r}	Rolling moment coefficient due to yaw rate $C_{l_r} = \frac{\partial C_l}{\partial \left(\frac{rb}{2V}\right)}$ (per radian)
$C_{l_{\delta_a}}$	Rolling moment coefficient due to aileron deflection $C_{l_{\delta_a}} = \frac{\partial C_l}{\partial \delta_a}$ (per degree)
$C_{l_{\delta_r}}$	Rolling moment coefficient due to rudder deflection $C_{l_{\delta_r}} = \frac{\partial C_l}{\partial \delta_r}$ (per degree)
C_m	Pitching moment coefficient $C_m = \frac{m}{\bar{q}S\bar{c}}$
C_{m_α}	Pitching moment coefficient due to angle-of-attack $C_{m_\alpha} = \frac{\partial C_m}{\partial \alpha}$ (per degree)
$C_{m_{\dot{\alpha}}}$	Pitching moment coefficient due to rate of change of angle-of-attack $C_{m_{\dot{\alpha}}} = \frac{\partial C_m}{\partial \left(\frac{\dot{\alpha}\bar{c}}{2V}\right)}$ (per radian)
$C_{m_{\delta_e}}$	Pitching moment coefficient due to elevator deflection $C_{m_{\delta_e}} = \frac{\partial C_m}{\partial \delta_e}$ (per degree)
C_{m_q}	Pitching moment coefficient due to pitch rate $C_{m_q} = \frac{\partial C_m}{\partial \left(\frac{q\bar{c}}{2V}\right)}$ (per radian)
C_N	Normal force coefficient $C_N = \frac{N}{\bar{q}S}$
C_{N_α}	Normal force coefficient due to angle-of-attack $C_{N_\alpha} = \frac{\partial C_N}{\partial \alpha}$ (per degree)
$C_{N_{\dot{\alpha}}}$	Normal force coefficient due to rate of change of angle-of-attack $C_{N_{\dot{\alpha}}} = \frac{\partial C_N}{\partial \left(\frac{\dot{\alpha}\bar{c}}{2V}\right)}$ (per radian)
$C_{N_{\delta_e}}$	Normal force coefficient due to elevator deflection $C_{N_{\delta_e}} = \frac{\partial C_N}{\partial \delta_e}$ (per degree)
C_{N_q}	Normal force coefficient due to pitch rate $C_{N_q} = \frac{\partial C_N}{\partial \left(\frac{q\bar{c}}{2V}\right)}$ (per radian)
C_n	Yawing moment coefficient $C_n = \frac{n}{\bar{q}Sb}$
C_{n_β}	Yawing moment coefficient due to angle-of-sideslip $C_{n_\beta} = \frac{\partial C_n}{\partial \beta}$ (per degree)
C_{n_p}	Yawing moment coefficient due to roll rate $C_{n_p} = \frac{\partial C_n}{\partial \left(\frac{pb}{2V}\right)}$ (per radian)
C_{n_r}	Yawing moment coefficient due to yaw rate $C_{n_r} = \frac{\partial C_n}{\partial \left(\frac{rb}{2V}\right)}$ (per radian)

$C_{n_{\delta_a}}$ Yawing moment coefficient due to aileron deflection
$C_{n_{\delta_a}} = \frac{\partial C_n}{\partial \delta_a}$ (per degree)

$C_{n_{\delta_r}}$ Yawing moment coefficient due to rudder deflection
$C_{n_{\delta_r}} = \frac{\partial C_n}{\partial \delta_r}$ (per degree)

C_X Longitudinal force coefficient
$C_X = \frac{X}{\bar{q}S}$

C_Y Side force coefficient
$C_Y = \frac{Y}{\bar{q}S}$

C_{Y_β} Side force coefficient due to angle-of-sideslip
$C_{Y_\beta} = \frac{\partial C_Y}{\partial \beta}$ (per degree)

C_{Y_p} Side force coefficient due to roll rate
$C_{Y_p} = \frac{\partial C_Y}{\partial \left(\frac{pb}{2V}\right)}$ (per radian)

C_{Y_r} Side force coefficient due to yaw rate
$C_{Y_r} = \frac{\partial C_Y}{\partial \left(\frac{rb}{2V}\right)}$ (per radian)

$C_{Y_{\delta_a}}$ Side force coefficient due to aileron deflection
$C_{Y_{\delta_a}} = \frac{\partial C_Y}{\partial \delta_a}$ (per degree)

$C_{Y_{\delta_r}}$ Side force coefficient due to rudder deflection
$C_{Y_{\delta_r}} = \frac{\partial C_Y}{\partial \delta_r}$ (per degree)

C_Z Vertical force coefficient
$C_Z = \frac{Z}{\bar{q}S}$

$\bar{c}$ Reference chord (1.65 m)

F Ratio of the regression mean square to the residual mean square

g Gravitational acceleration (9.81 m/s^2)

I_{XX} Roll moment of inertia (kg.m^2)

I_{YY} Pitch moment of inertia (kg.m^2)

I_{ZZ} Yaw moment of inertia (kg.m^2)

I_{XY} Cross product of moment of inertia (kg.m^2)

I_{XZ} Cross product of moment of inertia (kg.m^2)

I_{YZ} Cross product of moment of inertia (kg.m^2)

l Rolling moment (N.m)

M Mass of aircraft (kg)

m Pitching moment (N.m)

N Normal force (N)

n Yawing moment (N.m)

p Roll rate (rad/s)

q Pitch rate (rad/s)

$\bar{q}$ Dynamic pressure (N/m^2)

R^2 Squared multiple correlation coefficient

r Yaw rate (rad/s)

S Reference area (16.29 m^2)

V True velocity (m/s)

X Longitudinal force (N)

$x_{c.g.}$ Longitudinal *c.g.* position (m)

Y Side force (N)

$y_{c.g.}$ Lateral *c.g.* position (m)

Z Vertical force (N)

$z_{c.g.}$ Vertical *c.g.* position (m)

α	Angle-of-attack (°)
$\dot{\alpha}$	Time derivative of angle-of-attack (rad/s)
β	Angle-of-sideslip (°)
δ_a	Aileron deflection ($\delta_a = \delta_{a_L} - \delta_{a_R}$) (°)
δ_e	Elevator deflection (°)
δ_r	Rudder deflection (°)
θ	Pitch angle (°)
ϕ	Roll angle (°)
ψ	Yaw angle (°)
σ^2	Statistical variance

Subscripts

b	Body axes
$c.g.$	Centre-of-gravity
dep	Deployed
F	Fuel
GD	Gear down
L	Left (port)
mg	Main gear
ng	Nose gear
ret	Retracted
R	Right (starboard)
tot	Total

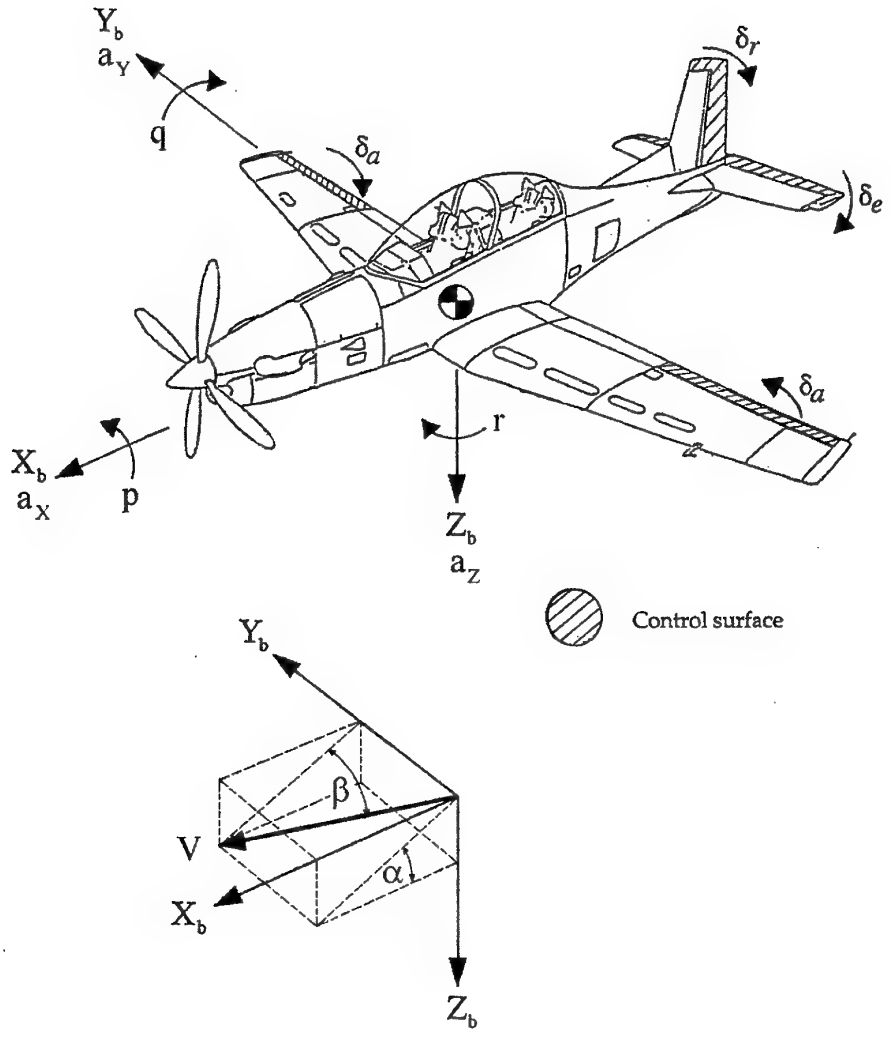

Aircraft sign convention and flow angle definitions (body axes).

Wing Reference Area (S)	16.29 m^2
Wing Span (b)	10.124 m
Mean Aerodynamic Chord ($\bar{c}$)	1.65 m

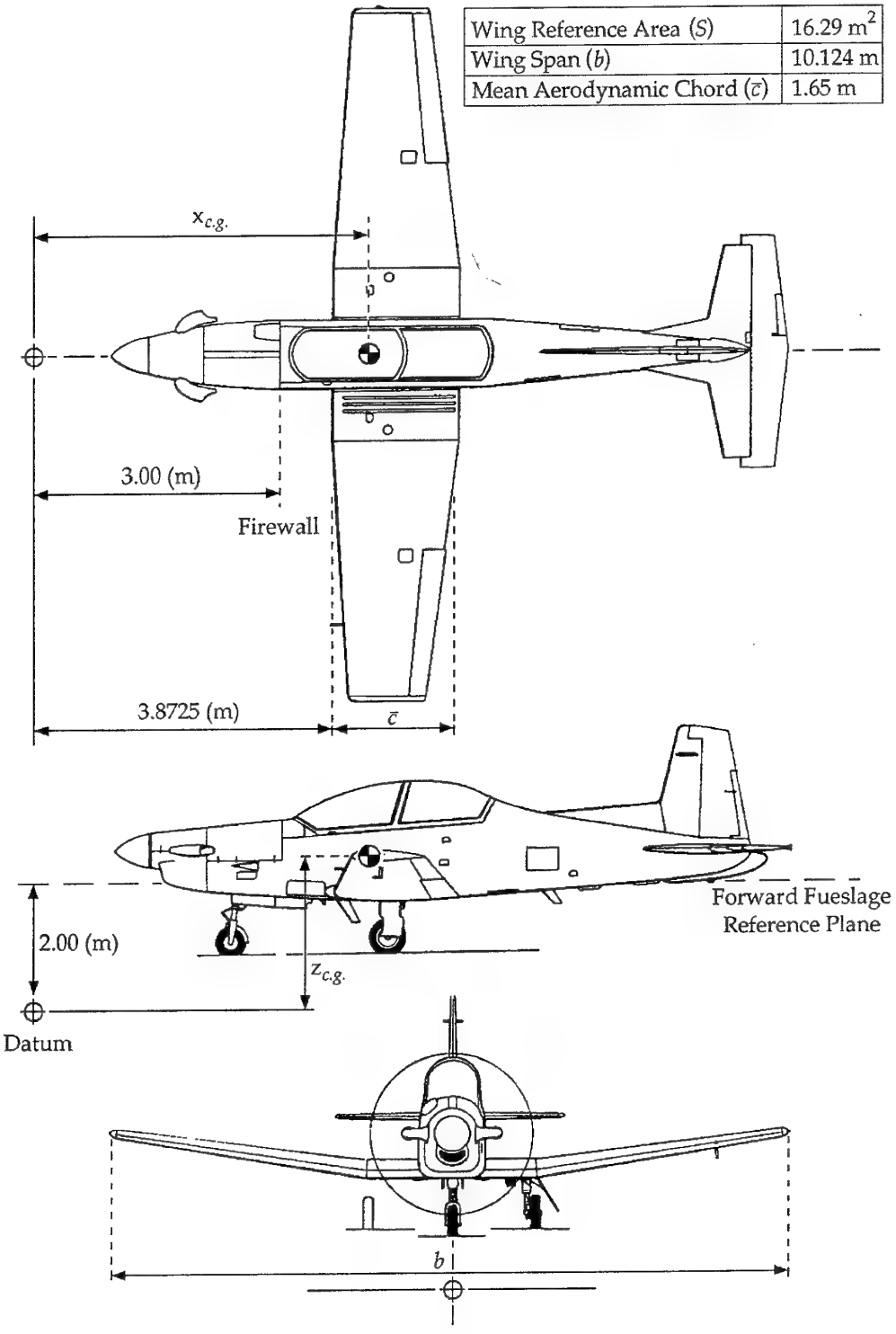

Aircraft Principle Dimensions.
(Numeric data sourced from Pilatus Structural Configuration Drawing 506.00.09.220F)

1 Introduction

The Pilatus PC 9/A is one of a number of high performance turbo-prop aircraft currently operated by the Royal Australian Air Force (RAAF). Work currently underway in the Air Operations Division (AOD) of the Defence Science and Technology Organisation (DSTO) includes investigations into the propeller power effects of such aircraft, and the PC 9/A was considered a suitable platform for study. A six degree-of-freedom flight dynamic model of the PC 9/A has been developed by AOD for use in these investigations, as well as for pilot-in-the-loop simulations in the Air Operations Simulation Centre and incident and accident investigations.

The development of a flight dynamic model requires information on the static and dynamic stability and control derivatives of the aircraft, as well as flight control laws and physical properties. The static data for the PC 9/A were collected during both power-off and power-on testing of a scaled aircraft model in the Aeronautical and Maritime Research Laboratory (AMRL) low-speed wind tunnel. Additional power-off static data were obtained from a computational fluid dynamic model for a limited number of aircraft configurations.

Flight test data for the PC 9/A was required to both validate the flight dynamic model and to provide dynamic derivative estimates of the aircraft. A flight test program was conducted on a PC 9/A aircraft, serial number A23-045, by the RAAF Aircraft Research and Development Unit (ARDU) between November 1998 and February 1999. The details of this flight test program and the aircraft instrumentation are reported in reference [5]. The estimation of the stability and control derivatives from the flight test data involved the use of system identification techniques, and required control input, aircraft response and flight condition data, measured using a high fidelity instrumentation system. Maximum likelihood and stepwise regression techniques were employed for the system identification. The longitudinal derivatives for the PC 9/A aircraft in cruise configuration determined using system identification techniques are reported in reference [1], while the lateral derivatives for the aircraft in cruise configuration are reported in reference [2].

This report presents the longitudinal and lateral stability and control derivatives of the PC 9/A extracted from flight test data for the approach and departure configurations, including a comparison with AMRL wind tunnel test data. Sections 2 and 3 present details of the test aircraft and instrumentation system. Section 4 presents the system identification techniques, while section 5 discusses the results.

2 PC 9/A Test Aircraft

2.1 Aircraft Description

The flight test aircraft, A23-045, is a Pilatus PC 9/A operated by ARDU. The PC 9/A is a single-engine, metal-skinned, low-wing, tandem two-seat training aircraft. The aircraft is powered by a Pratt and Whitney PT6A-62 turbo-prop engine flat rated to 950 SHP [3], which drives a Hartzell HC-D4N-2A four-blade variable pitch propeller. The aircraft was instrumented as outlined in section 3.

2.2 Flight Control System

The aircraft primary flight controls consist of the ailerons, rudder and elevator. The control surfaces are manually operated from a conventional dual control column and rudder pedal arrangement. The stick and rudder pedals are connected to the control surfaces through a system of control rods, bellcranks, cables and levers. Trimming control is provided on all three axes. The aircraft is fitted with trailing edge split flaps that cover the final 18% of the wing chord from the wing root to the inboard edge of the aileron. These flaps have three discrete positions, retracted ($\delta_f = 0°$), take-off ($\delta_f = 23°$), and landing ($\delta_f = 50°$). Additionally, the aircraft is fitted with a perforated flat plate airbrake that is located under the centre fuselage between the wing flaps. This airbrake is either retracted or deployed at an angle of 50°.

2.3 Weight, Centre-of-Gravity and Mass Moments-of-Inertia

The test aircraft, A23-045, was weighed, in clean configuration, by ARDU prior to the flight tests and had a basic mass of 1784.5 kg and a longitudinal centre-of-gravity position of 26.25% Mean Aerodynamic Chord (MAC) [4]. During the flight test program, the aircraft weight, centre-of-gravity and mass moments-of-inertia varied with fuel usage. Equations for the mass, centre-of-gravity, and mass moments-of-inertia of the clean aircraft are documented in [1, Appendix A]. These equations were used for analysis of flight test cases with airbrake deployed. Appendix A develops equations for the mass, centre-of-gravity, and mass moments-of-inertia of the aircraft in approach and departure configurations.

3 Instrumentation

Aircraft A23-045 was fitted with an instrumentation system designed specifically for the gathering of flight dynamic data. A summary of the instrumentation used in the flight test program is included below and a more comprehensive description of the design requirements and calibration is included in references [5] and [6]. The ARDU General Data Acquisition System (GDAS) was fitted in place of the rear ejection seat. The data were encoded by a 16-bit pulse code modulation system and were recorded onboard the aircraft using a MARS-2000 14-track tape. Real-time flight test monitoring was provided by telemetry data transmitted to the ARDU Primary Analysis Processor (PAP) hut.

The angular rates (p, q, r) and linear accelerations (a_X, a_Y, a_Z) were measured using the ARDU KAISG1134-1 Motion Platform. This consisted of three Smith Industries 950 RGS angular rate gyros and three SunStrand QA1400 servo accelerometers. The aircraft roll, pitch and yaw attitude angles (ϕ, θ, ψ) were obtained by tapping output from the existing LISA 2000A Artificial Horizon Reference System (AHRS).

Static outside air temperature (OAT), indicated airspeed (IAS), angle-of-attack (α) and angle-of-sideslip (β) were obtained from the Rosemount Model 92AN flight test air data boom, mounted on the outboard hardpoint on the starboard wing (see figure 1). Aileron

and elevator deflections were measured using Space Age Control Inc. series 160 cable position transducers. Rudder deflection was measured using a type 26V-11CX4C position transducer. All sensors were calibrated prior to commencement of the flight test program.

The aircraft was also instrumented to measure engine torque, propeller speed, inlet turbine temperature (ITT), gas generator speed (NG), fuel flow and fuel quantity. The torque, propeller speed, altitude and true airspeed, when used in conjunction with a performance map for the Hartzell HC-D4N-2A propeller [7], allowed the calculation of engine thrust.

4 Methods of Analysis

During the approach and departure phase of flight test program, doublet manoeuvres were performed about steady flight conditions at airspeeds between 120 and 200 KIAS. Reference [5] describes these manoeuvres in detail. The 25 longitudinal and 27 lateral doublet manoeuvres, for the aircraft in approach or departure configurations, were analysed using stepwise regression [8] and maximum likelihood estimation techniques [9] to determine the longitudinal and lateral stability and control derivatives of the aircraft.

Aircraft derivatives estimated from AMRL power-off wind tunnel tests [10] were used to provide comparisons for the static aircraft derivatives and, in the case of the maximum likelihood analysis, to provide *a priori* estimates to increase the rate of convergence of the system identification. Due to the lack of dynamic derivative estimates for the aircraft in approach or departure configurations, empirical estimates of the clean aircraft dynamic derivatives were used as *a priori* values to improve convergence.

A right handed orthogonal axes system was adopted for the analysis of the flight test data. Positive control surface deflections were defined as elevator trailing edge down, rudder trailing edge to port, and starboard aileron trailing edge down, port aileron trailing edge up.

4.1 Stepwise Regression

Stepwise regression is an unbiased least squares estimator in which new independent variables are inserted into a model, one at a time, until the regression equation is deemed acceptable. The appropriateness of the model can be determined by examining a number of quantities including the squared multiple correlation coefficient and the F statistic. The squared multiple correlation coefficient, R^2, gives a measure of the importance of each variable as it is inserted into the equation [8]; however, the improvement in R^2 due to the addition of new terms must have some real significance besides simply reflecting the inclusion of more terms. This can be determined by monitoring the F statistic, the ratio of the regression mean square to the residual mean square. The inclusion of any significant terms is generally accompanied by an increase in the F statistic and the best fit with the least number of parameters may be obtained by maximising F. Any variable which does not make a significant contribution is removed from the model, with the selection process continuing until no new variables remain to be inserted into the equation. Whilst stepwise regression gives estimates of the derivatives included in the regression equation, it also

permits a suitable structure for the model to be determined. In addition, it provides an independent check on the data estimated using the maximum likelihood technique.

The stepwise regression technique was applied using code available in the MATLAB© Statistics Toolbox [11]. The following model equations were identified during the analysis.

$$C_N = C_{N_0} + C_{N_\alpha}\alpha + C_{N_{\delta_e}}\delta_e \tag{1}$$

$$C_m = C_{m_0} + C_{m_\alpha}\alpha + C_{m_q}\frac{q\bar{c}}{2V} + C_{m_{\delta_e}}\delta_e \tag{2}$$

$$C_Y = C_{Y_0} + C_{Y_\beta}\beta + C_{Y_{\delta_r}}\delta_r \tag{3}$$

$$C_n = C_{n_0} + C_{n_\beta}\beta + C_{n_p}\frac{pb}{2V} + C_{n_r}\frac{rb}{2V} + C_{n_{\delta_r}}\delta_r \tag{4}$$

$$C_l = C_{l_0} + C_{l_\beta}\beta + C_{l_p}\frac{pb}{2V} + C_{l_r}\frac{rb}{2V} + C_{l_{\delta_a}}\delta_a \tag{5}$$

4.1.1 Error Band

Included in the stepwise regression analysis is the calculation of an error band on the estimated derivatives. For a confidence interval of 95%, this error band is approximately equal to two standard deviations. Figures 2 to 19 show the stepwise regression derivative estimates, including the calculated error band.

4.2 Maximum Likelihood

The maximum likelihood estimation technique was applied using the computer program, pEst, developed at NASA Dryden Flight Research Center [12]. pEst is an interactive parameter estimation program which solves a vector set of time-varying, ordinary differential equations of motion.

The longitudinal derivatives identified using the maximum likelihood technique are given in table 1. Three aerodynamic derivatives used in the longitudinal flight dynamic model were not identified due to difficulties in estimation and their small contribution.

The derivative $C_{m_{\dot{\alpha}}}$ is difficult to estimate from standard flight test manoeuvres and is usually considered as an additional component of the pitch damping derivative C_{m_q} during parameter identification [13]. Experience gained during the analysis of F-111C flight test

	Normal Force	Pitching Moment
Aerodynamic	C_{N_α}	C_{m_α} C_{m_q}
Control	$C_{N_{\delta_e}}$	$C_{m_{\delta_e}}$

Table 1: Longitudinal derivatives estimated.

data [14] has shown that it is preferable to fix $C_{m_{\dot{\alpha}}}$ at it's *a priori* value, chosen here as -7.823 (per radian), and allow C_{m_q} to be estimated.

Difficulties also arise when trying to estimate both the normal force due to pitch rate derivative, C_{N_q}, and the normal force due to the time rate-of-change of angle-of-attack derivative, $C_{N_{\dot{\alpha}}}$. Previous analysis of the PC 9/A clean aircraft longitudinal data [1, Appendix B] has shown that the relative contributions of C_{N_q} and $C_{N_{\dot{\alpha}}}$ to the total aircraft normal force are negligible. Therefore, these derivatives have been fixed at their *a priori* values, chosen as 7.96 (per radian) and 3.061 (per radian), respectively, without any loss of accuracy of the estimation of the other normal force derivatives, C_{N_α} and $C_{N_{\delta_e}}$.

Due to a lack of empirical data for the PC 9/A in approach and departure configurations, the *a priori* values of $C_{m_{\dot{\alpha}}}$, C_{N_q} and $C_{N_{\dot{\alpha}}}$, used during the data analysis, are the clean aircraft values obtained from reference [15]. The resulting total force and moment coefficient equations used in the longitudinal state and response equations for the maximum likelihood analysis of the PC 9/A are given in equations 6 and 7.

$$C_N = C_{N_0} + C_{N_\alpha}\alpha + 7.96\frac{q\bar{c}}{2V} + C_{N_{\delta_e}}\delta_e + 3.061\frac{\dot{\alpha}\bar{c}}{2V} \tag{6}$$

$$C_m = C_{m_0} + C_{m_\alpha}\alpha + C_{m_q}\frac{q\bar{c}}{2V} + C_{m_{\delta_e}}\delta_e - 7.823\frac{\dot{\alpha}\bar{c}}{2V} \tag{7}$$

The lateral derivatives identified using the maximum likelihood technique are given in table 2.

	Side Force	Yawing Moment	Rolling Moment
Aerodynamic	C_{Y_β}	C_{n_β} C_{n_p} C_{n_r}	C_{l_β} C_{l_p} C_{l_r}
Control	$C_{Y_{\delta_r}}$	$C_{n_{\delta_r}}$	$C_{l_{\delta_a}}$

Table 2: Lateral derivatives estimated.

Five aerodynamic derivatives used in the lateral flight dynamic model were not identified due to both their small contribution and difficulty of estimation. C_{Y_p} was fixed at a value of -0.16 (per radian), C_{Y_r} at 0.34 (per radian), $C_{Y_{\delta_a}}$ at 0.0 (per degree), $C_{n_{\delta_a}}$ at -0.000035 (per degree) and $C_{l_{\delta_r}}$ remained fixed at 0.0035 (per degree). As for the longitudinal case,

a lack of approach and departure configuration empirical data required the use of clean aircraft *a priori* values for C_{Y_p}, C_{Y_r}, $C_{Y_{\delta_a}}$, $C_{Y_{\delta_r}}$ and $C_{l_{\delta_r}}$, obtained from references [16] and [15]. The resulting total force and moment coefficient equations used in the lateral state and response equations for the maximum likelihood analysis of the PC 9/A are given in equations 8, 9 and 10. The differences between equations 1, 2, 3, 4 and 5, and 6, 7, 8, 9 and 10 are important, and arise from the inclusion of the *a priori* values in the maximum likelihood technique.

$$C_Y = C_{Y_0} + C_{Y_\beta}\beta - 0.1608\frac{pb}{2V} + 0.3417\frac{rb}{2V} + C_{Y_{\delta_r}}\delta_r \tag{8}$$

$$C_n = C_{n_0} + C_{n_\beta}\beta + C_{n_p}\frac{pb}{2V} + C_{n_r}\frac{rb}{2V} - 0.000035\delta_a + C_{n_{\delta_r}}\delta_r \tag{9}$$

$$C_l = C_{l_0} + C_{l_\beta}\beta + C_{l_p}\frac{pb}{2V} + C_{l_r}\frac{rb}{2V} + C_{l_{\delta_a}}\delta_a + 0.003491\delta_r \tag{10}$$

4.2.1 Cramer-Rao Bounds

For the estimated parameters, pEst calculates a measure of the estimation certainty known as the Cramer-Rao bound. A detailed interpretation of this quantity is given in [17]. The Cramer-Rao bounds are shown for each derivative estimated by pEst in figures 2 to 19. The Cramer-Rao bounds have been factored in accordance with the procedures described in [17] to account for the presence of band-limited noise.

5 Results and Discussion

Longitudinal and lateral derivatives estimated via maximum likelihood parameter estimation, stepwise regression, and power-off wind tunnel experiments are summarised in figures 2 to 19. Data are presented for the aircraft with gear down, take-off flap with gear down, landing flap with gear down, and clean with airbrake extended.

5.1 Angle-of-Attack Derivatives

Figures 2 to 4 show the angle-of-attack derivatives C_{N_α} and C_{m_α} plotted against α. The flight test estimates of C_{N_α} are generally in good agreement with wind tunnel estimates. The maximum likelihood estimates are higher than the stepwise regression estimates and there is an increase in the Cramer-Rao bounds of the estimates as flap deflection is increased, indicating increased uncertainty. This is discussed in more detail in section 5.9.

The flight test estimates of pitch stiffness, C_{m_α}, are consistently smaller in magnitude than the wind tunnel estimates, which are power-off. This difference is due to the imbalance

between two competing effects acting on the portion of the horizontal tail within the propeller slipstream, these being the increased dynamic pressure and the reduced angle of incidence. The reduction in angle of incidence dominates, resulting in an overall reduction in the pitch stiffness of the aircraft. This phenomenon is discussed in more detail in reference [1]. The stepwise regression estimates are consistently smaller in magnitude than the maximum likelihood estimates. The small Cramer-Rao bounds indicate a high level of confidence in the maximum likelihood estimates.

5.2 Pitch Rate Derivatives

Figures 2 to 4 show the pitch rate derivative, C_{m_q}, plotted against α. As discussed earlier, $C_{m_{\dot{\alpha}}}$ was fixed at it's *a priori* value to aid the estimation of the pitch damping derivative C_{m_q}. This method has been used successfully during other parameter estimation exercises [14], and was verified as suitable for use with the PC 9/A flight testing in reference [1].

The AMRL low-speed wind tunnel has no facility to measure dynamic derivatives, and empirical data was not available for the Pilatus PC 9/A in approach or departure configurations. Figures 2 to 4 show that the maximum likelihood estimates are smaller in magnitude than the stepwise regression estimates, and that the Cramer-Rao bounds and difference between maximum likelihood and stepwise regression estimates increases as flap deflection increases.

5.3 Longitudinal Control Derivatives

Figures 5 to 7 show the longitudinal control derivatives, $C_{m_{\delta_e}}$ and $C_{N_{\delta_e}}$, plotted against α. The maximum likelihood estimates of $C_{m_{\delta_e}}$ agree very closely with wind tunnel estimates for all configurations. The stepwise regression estimates are smaller in magnitude. Small Cramer-Rao bounds indicate high confidence in the estimates, although they increase with increasing flap deflection.

Estimates of $C_{N_{\delta_e}}$ show only a small amount of scatter for all configurations. Maximum likelihood estimates are positive, and just below the wind tunnel estimates, while stepwise regression estimates are negative. As discussed previously, *a priori* values are included in the maximum likelihood technique, whereas the stepwise regression technique does not consider these values. Analysis of the effect of inclusion or exclusion of the *a priori* values [1] demonstrated a change in sign of the maximum likelihood estimates of $C_{N_{\delta_e}}$. It was therefore theorised that the effect of setting both $C_{N_{\dot{\alpha}}}$ and C_{N_q} to zero is to reduce the rate of onset of normal force during a manoeuvre and therefore, the modelling techniques decrease the value of $C_{N_{\delta_e}}$, to below zero, to compensate. This ensures the overall match of the data is good but results in some loss of model resolution during the initial application of elevator [1].

5.4 Angle-of-Sideslip Derivatives

Figures 8 to 10 show the angle-of-sideslip derivatives C_{Y_β}, C_{n_β} and C_{l_β} plotted against α. The flight test estimates of C_{Y_β} are greater in magnitude than the wind tunnel estimates, and the difference between flight test and wind tunnel increases with flap deflection. The Cramer-Rao bounds also increase with flap deflection. In general, the stepwise regression estimates are smaller in magnitude than the maximum likelihood estimates.

Flight test estimates of the directional stability derivative, C_{n_β}, show good agreement between the stepwise regression and maximum likelihood techniques for the gear down cases, but a slight divergence between the two techniques as flap deflection is increased. Both flight test estimation techniques yield values significantly below that measured in the wind tunnel, which is power-off. This difference is due to the imbalance between two competing effects acting on the portion of the vertical tail within the propeller slipstream, these being the increased dynamic pressure and the decreased angle of incidence. The reduction in angle of incidence dominates, resulting in an overall reduction in the directional stability of the aircraft.

The flight test estimates of the dutch roll derivative, C_{l_β}, show good agreement with wind tunnel for all configurations. There is a increase in scatter and Cramer-Rao bound magnitude with increasing flap deflection.

5.5 Yaw Rate Derivatives

The yaw rate derivatives, C_{n_r} and C_{l_r}, are plotted against α in figures 11 to 13. The AMRL low-speed wind tunnel has no facility to measure dynamic derivatives, and empirical data was not available for the Pilatus PC 9/A in approach or departure configurations. As mentioned previously, C_{Y_r} was constrained to its *a priori* value for the maximum likelihood analysis, and not estimated in the stepwise regression analysis. Investigations have previously been undertaken [2, Appendix B] to assess the relative contribution of each derivative to the aircraft's forces and moments to ensure that those set to their *a priori* values were small contributors. This analysis showed the yaw rate contribution to side force to be small.

Flight test estimates of yawing moment due to yaw rate derivative, C_{n_r}, show good agreement between the maximum likelihood and stepwise regression techniques for all configurations. Further, the small Cramer-Rao bounds indicate a high degree of confidence in the estimate, despite the lack of corroborating data. The figures show a general decrease in the average magnitude of C_{n_r} as flap deflection is increased.

The rolling moment due to yaw rate, C_{l_r}, whilst being small, is an important lateral-directional cross-coupling derivative. Flight test estimates of C_{l_r} show the same trends as C_{n_r}; small Cramer-Rao bounds indicating a high level of confidence in the estimate, and a general decrease in the magnitude of the estimate with increasing flap deflection.

5.6 Roll Rate Derivatives

Figures 14 to 16 show the roll rate derivatives, C_{n_p} and C_{l_p}, plotted against α. The side force due to roll rate, C_{Y_p}, is a small derivative and was not estimated in stepwise regression or maximum likelihood analysis.

The yawing moment due to roll rate derivative, C_{n_p}, is an important lateral-directional cross-coupling term. Maximum likelihood and stepwise regression estimates show good agreement with low Cramer-Rao bounds and little scatter. The average magnitude of C_{n_p} decreases as flap deflection increases.

The roll damping derivative, C_{l_p}, estimates from maximum likelihood and stepwise regression show good agreement, with small Cramer-Rao bounds. The magnitude of C_{l_p} does not change significantly with configuration.

5.7 Lateral Control Derivatives

Figures 17 to 19 show the lateral control derivatives, $C_{Y_{\delta_r}}$, $C_{n_{\delta_r}}$, and $C_{l_{\delta_a}}$, plotted against α. The yawing moment due to aileron derivative, $C_{n_{\delta_a}}$, and rolling moment due to rudder derivative, $C_{l_{\delta_r}}$, are both small derivatives which were not estimated in either stepwise regression or maximum likelihood analyses.

Flight test estimates of $C_{Y_{\delta_r}}$ show a higher degree of scatter than is present in estimates of any other derivative, but are centred on the wind tunnel estimate. The maximum likelihood estimates have sizeable Cramer-Rao bounds, indicating a reduced level of confidence in the estimates, while the stepwise regression estimates have quite small error bands. There is a general increase in scatter and Cramer-Rao bound magnitude with increasing flap deflection.

Estimates of the rudder effectiveness derivative, $C_{n_{\delta_r}}$, show small Cramer-Rao bounds and error bands, indicating a high level of confidence in the estimates, and little scatter. Both maximum likelihood and stepwise regression estimates are larger in magnitude than the wind tunnel estimates. There is no significant change in the estimated value of $C_{n_{\delta_r}}$ with aircraft configuration.

Estimates of the aileron effectiveness derivative, $C_{l_{\delta_a}}$, show little scatter, and only a small increase in Cramer-Rao bounds with increasing flap deflection. Both maximum likelihood and stepwise regression techniques provide estimates that are consistently larger in magnitude than the wind tunnel estimates, this difference tending to increase with increasing flap deflection.

5.8 Variation of Derivatives with Airbrake Deployment

The effect of deployment of the aircraft's airbrake on the aerodynamic characteristics of the aircraft was assessed by conducting longitudinal and lateral doublet manoeuvres with the aircraft in clean configuration and airbrake extended. Only eight flight test manoeuvres were performed, and therefore, the results from maximum likelihood and

stepwise regression techniques are presented as averaged values. These are compared with average values for the clean aircraft in tables 3 to 4.

Derivative	Airbrake (Maximum Likelihood)	Airbrake (Stepwise)	Clean Aircraft
C_{N_α}	9.23E-2	8.59E-2	8.53E-2
C_{m_α}	-6.28E-3	-4.92E-3	-6.53E-3
C_{m_q}	-1.57E+1	-1.95E+1	-1.53E+1
$C_{N_{\delta_e}}$	1.19E-3	-4.67E-3	1.42E-4
$C_{m_{\delta_e}}$	-2.18E-2	-2.02E-2	-1.93E-2

Table 3: Comparison of averaged longitudinal flight test derivatives with airbrake deployed, using maximum likelihood and stepwise regression techniques, to averaged clean aircraft results [1].

Derivative	Airbrake (Maximum Likelihood)	Airbrake (Stepwise)	Clean Aircraft
C_{Y_β}	-1.65E-2	-1.52E-2	-1.32E-2
C_{n_β}	1.68E-3	1.94E-3	1.44E-3
C_{l_β}	-1.45E-3	-1.30E-3	-1.40E-3
C_{n_r}	-1.68E-1	-2.03E-1	-2.11E-1
C_{l_r}	1.32E-1	1.24E-1	1.37E-1
C_{n_p}	-3.46E-2	-2.36E-2	-5.56E-2
C_{l_p}	-4.85E-1	-4.45E-1	-4.75E-1
$C_{Y_{\delta_r}}$	2.03E-3	1.72E-3	3.38E-3
$C_{n_{\delta_r}}$	-1.81E-3	-1.90E-3	-1.90E-3
$C_{l_{\delta_a}}$	-1.69E-3	-1.68E-3	-1.73E-3

Table 4: Comparison of averaged lateral flight test derivatives with airbrake deployed, using maximum likelihood and stepwise regression techniques, to averaged clean aircraft results [2].

The deployment of the airbrake could be expected to have its most significant impact in terms of an incremental addition to the pitching moment and axial force coefficients, with little impact on the associated derivatives. However, inspection of tables 3 and 4 show some interesting trends. Table 3 shows an increase in magnitude of C_{N_α}, C_{m_q} and $C_{m_{\delta_e}}$, and a decrease in magnitude of C_{m_α}, with airbrake deployment. The other longitudinal derivative, $C_{N_{\delta_e}}$, is not consistently affected by airbrake deployment. Table 4 shows an increase in magnitude of both C_{Y_β} and C_{n_β}; a decrease in magnitude of the yaw damping term C_{n_r}; and a significant decrease in magnitude of C_{n_p} and $C_{Y_{\delta_r}}$.

The changes in the lateral stability and control derivatives are particularly interesting, in that airbrake deployment would not intuitively be expected to have a significant impact on them. The increase in magnitude of C_{Y_β} is a result of the increase in side area of the aircraft when it is yawed with the airbrake deployed. The increase in magnitude of the directional stability term, C_{n_β}, then follows because the airbrake is located aft of

the centre-of-gravity, and therefore, the side force will cause a restorative moment. The decrease in yaw damping, C_{n_r}, can not be attributed directly to the forces and moments generated by the airbrake, but rather to its influence on the flow over the aircraft's ventral fin. Deployment of the airbrake will significantly disturb the airflow downstream. Hence the ventral fin ,which is located behind the airbrake on the underside of the fuselage, will experience reduced authority. Whilst there is a significant decrease in the magnitude of C_{n_p} this derivative has only a small impact on the overall handling of the aircraft and hence any changes will be relatively insignificant. The most interesting lateral change due to airbrake deployment is the reduction in side force due to rudder derivative, $C_{Y_{\delta_r}}$, and the fact that this is not accompanied by a similar decrease in the rudder control power, $C_{n_{\delta_r}}$. This result suggests that while the side force for a given rudder deflection is reduced, the moment it produces about the aircraft centre-of-gravity is not, a result that is not intuitive.

5.9 Configuration and Altitude Dependency

Figures 2 to 19 show graphically, and tables 6 to 9 summarise, the longitudinal and lateral derivatives estimated from flight test for the Pilatus PC 9/A in three configurations: gear deployed, gear deployed with take-off flap, and gear deployed with landing flap.

Figures 2 to 4 show an increase in the Cramer-Rao bound magnitude with increasing flap deflection, particularly in plots of C_{N_α}. An analysis of the signal variance for the α, a_Z, β, and a_Y flight test data channels was performed by filtering each data channel using the 'filtfilt' function in MATLAB©. The variance of the original data channels was then calculated by comparison to the filtered data. The results of this analysis, averaged over all manoeuvres, are summarised in table 5 as ratios of the signal variance for each configuration to the signal variance for the gear down configuration ($\frac{\sigma^2}{\sigma^2_{GD}}$).

	α	a_Z	β	a_Y
Gear down	1.00	1.00	1.00	1.00
Take-off flap	1.37	1.06	2.15	2.84
Landing flap	3.49	3.71	7.54	9.05

Table 5: Signal variance ratios for gear down, take-off flap, and landing flap configurations.

Inspection of the table shows that the variance ratio of the flight test data increases with increasing flap deflection, up to a maximum factor of 9 for a_Y with landing flap. This increase in signal variance with flap deflection can be attributed to the design of the flaps on the PC 9/A. The aircraft is fitted with split trailing edge flaps, such that as flap deflection increases, large areas of separated flow are produced at the wing trailing edge. This turbulent separated flow buffets the empennage of the aircraft causing the whole airframe to vibrate. It is these vibrations that result in the variance shown in the flight test measured data. The increase in variance of the flight test data manifests itself as an increase in the Cramer-Rao bounds of the flight test estimates in two ways. In the case of the α and β signals, the data are used directly by the maximum likelihood technique and as such will influence the quality of the model response. For the acceleration signals, the

data are used for comparison with the calculated model response, and as such any variance will manifest itself as an increase in error between the model and the flight test and hence an increased Cramer-Rao bound. The stepwise regression technique is not affected in the same way by signal variance.

Plots of C_{Y_β} in figures 8 to 10 show a divergence between flight test and wind tunnel estimates as flap deflection is increased. The trend, which is present in some other derivatives to a lesser extent, could be the result of several factors. As described previously, the increased flow separation, and associated impacts on the flight data, that occur when flaps are deflected could lead to errors in the flight test estimated value of derivatives.

Tables 6 to 9 show the mean values across the linear angle-of-attack range (0° – 6°) of the aerodynamic derivatives estimated by both maximum likelihood and stepwise regression techniques, for each configuration and altitude band.

	Gear Down 5000 ft	Gear Down 15 000 ft	Take-off Flap 5 000 ft	Take-off Flap 15000 ft	Landing Flap 5 000 ft	Landing Flap 15 000 ft
C_{N_α}	8.83E-2	8.62E-2	9.51E-2	9.16E-2	9.40E-2	9.35E-2
C_{m_α}	-1.03E-2	-9.08E-3	-1.15E-2	-1.01E-2	-1.00E-2	-9.41E-3
C_{m_q}	-1.54E+1	-1.61E+1	-1.14E+1	-1.29E+1	-1.49E+1	-1.68E+1
$C_{N_{\delta_e}}$	2.62E-3	1.62E-3	2.99E-3	2.60E-3	1.37E-3	1.63E-3
$C_{m_{\delta_e}}$	-2.34E-2	-2.31E-2	-2.32E-2	-2.42E-2	-2.36E-2	-2.51E-2

Table 6: Summary of longitudinal derivatives estimated using maximum likelihood.

	Gear Down 5000 ft	Gear Down 15 000 ft	Take-off Flap 5 000 ft	Take-off Flap 15000 ft	Landing Flap 5 000 ft	Landing Flap 15 000 ft
C_{N_α}	8.32E-2	8.52E-2	9.07E-2	8.60E-2	8.63E-2	8.26E-2
C_{m_α}	-8.75E-3	-7.92E-3	-8.80E-3	-8.42E-3	-7.87E-3	-7.92E-3
C_{m_q}	-1.74E+1	-1.62E+1	-1.58E+1	-1.70E+1	-1.77E+1	-1.88E+1
$C_{N_{\delta_e}}$	-4.23E-3	-4.23E-3	-5.15E-3	-2.75E-3	-4.50E-3	-3.55E-3
$C_{m_{\delta_e}}$	-1.90E-2	-1.78E-2	-2.00E-2	-2.12E-2	-1.99E-2	-2.06E-2

Table 7: Summary of longitudinal derivatives estimated by stepwise regression.

The flight test estimates of the longitudinal derivatives in general show no significant trend with configuration, with the exception that the maximum likelihood estimates of $C_{N_{\delta_e}}$ and $C_{m_{\delta_e}}$ show a decrease and increase in magnitude respectively with increasing flap deflection. However, many of the lateral derivative flight test estimates show definite trends with flap deflection. Estimates of C_{Y_β}, C_{n_β}, and $C_{Y_{\delta_r}}$ from both maximum likelihood and stepwise regression show an increase in magnitude with increasing flap deflection. Estimates of C_{n_p}, C_{n_r}, and C_{l_β} show a decrease in magnitude with flap deflection. The other lateral derivative estimates are not consistently and significantly affected by flap deflection. Figures 2 to 19 do not show any significant altitude dependency.

	Gear Down 5000 ft	Gear Down 15 000 ft	Take-off Flap 5 000 ft	Take-off Flap 15000 ft	Landing Flap 5 000 ft	Landing Flap 15 000 ft
C_{Y_β}	-1.75E-2	-1.73E-2	-2.05E-2	-1.96-2	-2.29E-2	-2.22E-2
C_{n_β}	1.59E-3	1.54E-3	2.01E-3	1.89E-3	2.18E-3	2.22E-3
C_{l_β}	-1.60E-3	-1.50E-3	-1.43E-3	-1.62E-3	-1.17E-3	-1.48E-3
C_{n_r}	-1.97E-1	-1.99E-1	-1.52E-1	-1.48E-1	-1.39E-1	-9.57E-2
C_{l_r}	1.91E-1	1.86E-1	5.79E-2	5.91E-2	1.05E-1	5.54E-2
C_{n_p}	-7.41E-2	-7.11E-2	-4.34E-2	-3.58E-2	-4.27E-2	-2.88E-2
C_{l_p}	-5.27E-1	-5.00E-1	-4.89E-1	-5.63E-1	-4.54E-1	-5.63E-1
$C_{Y_{\delta_r}}$	4.17E-3	4.41E-3	4.72E-3	4.97E-3	5.23E-3	7.54E-3
$C_{n_{\delta_r}}$	-2.12E-3	-2.05E-3	-2.01E-3	-1.82E-3	-1.99E-3	-1.98E-3
$C_{l_{\delta_a}}$	-1.90E-3	-1.78E-3	-1.94E-3	-2.04E-3	-1.90E-3	-2.05E-3

Table 8: Summary of lateral derivatives estimated using maximum likelihood.

	Gear Down 5000 ft	Gear Down 15 000 ft	Take-off Flap 5 000 ft	Take-off Flap 15000 ft	Landing Flap 5 000 ft	Landing Flap 15 000 ft
C_{Y_β}	-1.59E-2	-1.67E-2	-1.81E-2	-1.80E-2	-2.14E-2	-2.09E-2
C_{n_β}	1.67E-3	1.61E-3	2.09E-3	2.05E-3	2.32E-3	2.35E-3
C_{l_β}	-1.58E-3	-1.48E-3	-1.34E-3	-1.37E-3	-1.15E-3	-1.30E-3
C_{n_r}	-1.96E-1	-2.07E-1	-1.60E-1	-1.67E-1	-1.54E-1	-1.22E-1
C_{l_r}	1.20E-1	1.34E-1	1.17E-1	1.48E-1	1.27E-1	1.36E-1
C_{n_p}	-5.98E-2	-5.85E-2	-2.47E-2	-3.72E-2	-2.37E-2	-2.22E-2
C_{l_p}	-5.02E-1	-4.69E-1	-4.65E-1	-4.56E-1	-4.56E-1	-4.59E-1
$C_{Y_{\delta_r}}$	2.76E-3	2.78E-3	2.79E-3	2.99E-3	2.96E-3	2.92E-3
$C_{n_{\delta_r}}$	-2.14E-3	-2.09E-3	-2.04E-3	-2.10E-3	-2.07E-3	-2.06E-3
$C_{l_{\delta_a}}$	-1.90E-3	-1.78E-3	-1.92E-3	-1.89E-3	-1.92E-3	-1.95E-3

Table 9: Summary of lateral derivatives estimated by stepwise regression.

6 Conclusions

The longitudinal and lateral stability and control derivatives of the PC 9/A in approach and departure configurations have been determined from flight test data measurements using maximum likelihood and stepwise regression estimation techniques. Where available, comparisons have been made with derivative estimates from wind tunnel testing.

Flight test estimates of the normal force due to angle-of-attack derivative, C_{N_α} showed an increase in magnitude with increasing flap deflection, and good agreement with wind tunnel results for all configurations. Pitch stiffness derivative, C_{m_α}, estimates from flight test were consistently smaller in magnitude than wind tunnel results. However, the same trend, of increasing pitch stiffness with flap deflection, was demonstrated in flight test and wind tunnel. Flight test estimates of $C_{N_{\delta_e}}$ are scattered about zero, but in all cases are

less than the wind tunnel result. Maximum likelihood estimates of elevator effectiveness, $C_{m_{\delta_e}}$, match well with wind tunnel results for all configurations, while stepwise regression estimates are consistently smaller in magnitude. No wind tunnel or empirical results for pitch stiffness were available for comparison with flight test estimates. However, the flight test estimates show a general trend of decreasing pitch stiffness with increasing flap deflection.

Flight test estimates of angle-of-sideslip derivatives, C_{Y_β} and C_{l_β}, and rudder derivative, $C_{Y_{\delta_r}}$, show good agreement with wind tunnel estimates for all configurations. Flight test estimates of directional stability derivative, C_{n_β}, are consistently smaller in magnitude than the wind tunnel results, for all configurations. Flight test estimates of derivatives $C_{n_{\delta_r}}$ and $C_{l_{\delta_a}}$ are greater in magnitude than wind tunnel results. No wind tunnel or empirical data were available for comparison of lateral dynamic derivatives. However, rolling moment derivatives, C_{l_p} and C_{l_r} were largely unaffected by configuration changes, while yawing moment derivatives, C_{n_p} and C_{n_r}, demonstrated a trend of decreasing magnitude with increasing flap deflection.

In general, the flight test results showed no significant trend with altitude. However, all flight test estimated derivatives showed a trend of increased scatter and larger Cramer-Rao bounds with increasing flap deflection. Analysis of flight test data showed that this trend can be attributed to changes in signal variance due to increased airframe buffet with flap deployment.

Comparisons of flight test estimates of stability and control derivatives, with airbrake deployed, to those of the clean aircraft showed significant changes both longitudinally and laterally. However, the limited number of test manoeuvres performed in this configuration places a caveat on any conclusions drawn about the influence of the airbrake.

References

1. A. D. Snowden, H. A. Keating, N. van Bronswijk, and J. S. Drobik. A correlation between flight-determined longitudinal derivatives and ground based data for the Pilatus PC 9/A training aircraft in cruise configuration. Technical Report 0937, Air Operations Division, Aeronautical and Maritime Research Laboratory, Feb, 2000.

2. H. A. Keating, N. van Bronswijk, A. D. Snowden, and J. S. Drobik. A correlation between flight-determined lateral derivatives and ground based data for the Pilatus PC 9/A training aircraft in cruise configuration. Technical Report 0988, Air Operations Division, Aeronautical and Maritime Research Laboratory, Feb, 2000.

3. Royal Australian Air Force. *Flight Manual PC 9/A. Defence Instruction (Air Force) AAP 7212.007-1*, June 1989.

4. M.C. Sciberras. Aircraft weigh record – A23-045. ARDU 2501/60/TechPt1(5), November 1998.

5. A. D. Snowden. PC 9/A flight tests summary. Client Report AOD 99/01, Aeronautical and Maritime Research Laboratory, 1999.

6. B. A. Woodyatt, A. D. Snowden, and K. E. Lillingston. The development of a PC 9/A flight dynamic model validation flight test program. Client Report AOD 98/07, Aeronautical and Maritime Research Laboratory, 1998.

7. British Aerospace. Pilatus PC 9/A performance maps. Technical memorandum, British Aerospace Aerodynamics, Brough.

8. V. Klein. Estimation of aircraft aerodynamic parameters from flight data. *Progress in Aerospace Sciences*, 26:1–77, 1989.

9. R.E. Maine and K.W. Iliff. Application of parameter estimation to aircraft stability and control, the output error approach. Reference Publication 1168, NASA Dryden Flight Research Facility, Edwards, California, USA, June 1986.

10. R. M. Carmichael and B. A. Woodyatt. Estimates of the power-off aerodynamic characteristics of the Pilatus PC 9/A. Client Report AOD 96/29, Aeronautical and Maritime Research Laboratory, February 1997.

11. The MathWorks, Inc. *Statistics Toolbox User's Guide.* Natick, MA, January 1997.

12. J.E. Murray and R.E. Maine. pEst version 2.1 user's manual. Technical Memorandum 8828, NASA Ames Research Center, Dryden Flight Research Facility, Edwards, CA, USA, September 1987.

13. R.E. Maine and K.W. Iliff. Maximum likelihood estimation of translational acceleration derivatives from flight data. *AIAA Journal of Aircraft*, 1979.

14. A.D. Snowden and J.S. Drobik. F-111C longitudinal and lateral aerodynamic flight data analysis for take-off and landing configurations. Technical Report 0321, DSTO–Aeronautical and Maritime Research Laboratory, Melbourne, Victoria, Australia, April 1996.

15. PEI Aerodynamics. Evaluation of stability derivatives for the PC 9/A turbo-trainer. Technical report, Pilatus Aircraft Limited, 30 July 1983.

16. N. van Bronswijk. *Investigation of the Effects of Propeller Power on the Stability and Control of a Propeller Powered, Single-Engined, Low-Wing Monoplane.* PhD thesis, University of Sydney, In Preparation.

17. R.E. Maine and K.W. Iliff. User's manual for MMLE3, a general FORTRAN program for maximum likelihood parameter estimation. Technical Paper 1563, Dryden Flight Research Center, Edwards, California, USA, 1980.

18. I. Anderson and D. Mongru. Specification of the loading system for the PC 9/A fatigue test. Technical Report DSTO-TR-0259, Aeronautical and Maritime Research Laboratory, September 1995.

19. Structural configuration drawing 506.00.09.220 F, 27 January, 1983.

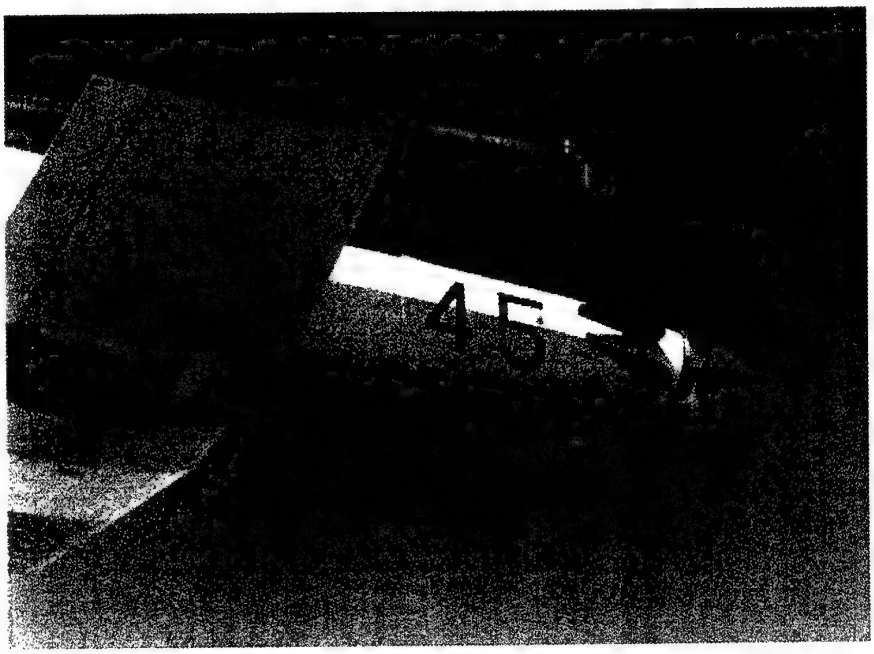

Figure 1: Air data boom installation.

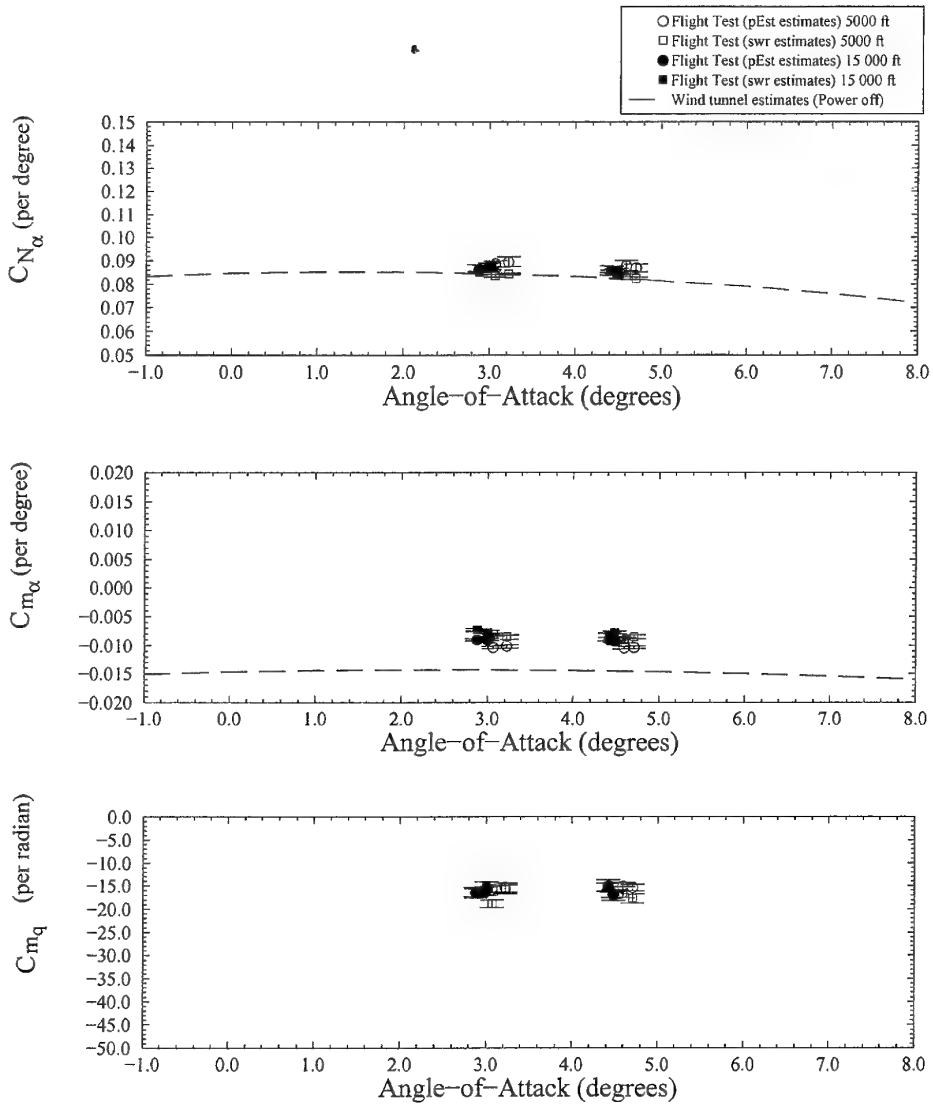

Figure 2: PC 9/A angle-of-attack and pitch rate derivatives, gear down.

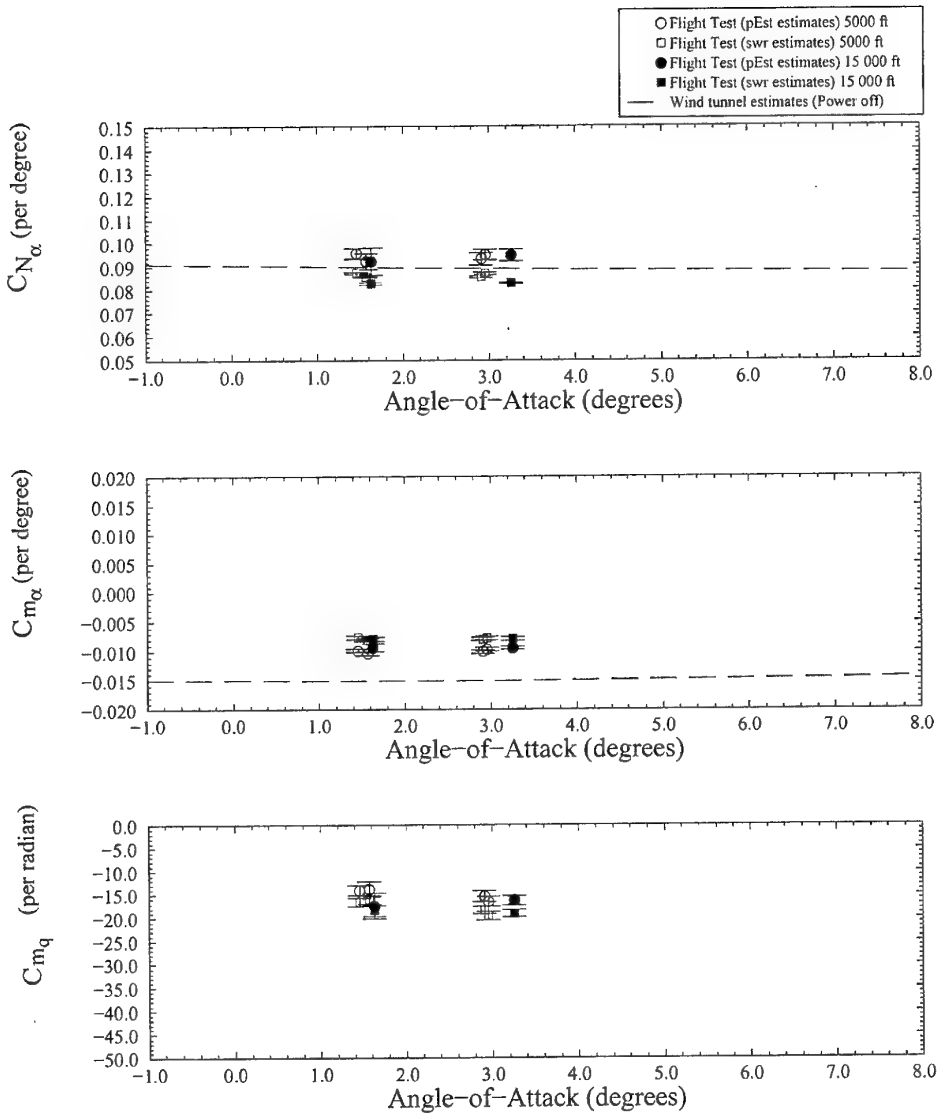

Figure 3: PC 9/A angle-of-attack and pitch rate derivatives, take-off flap.

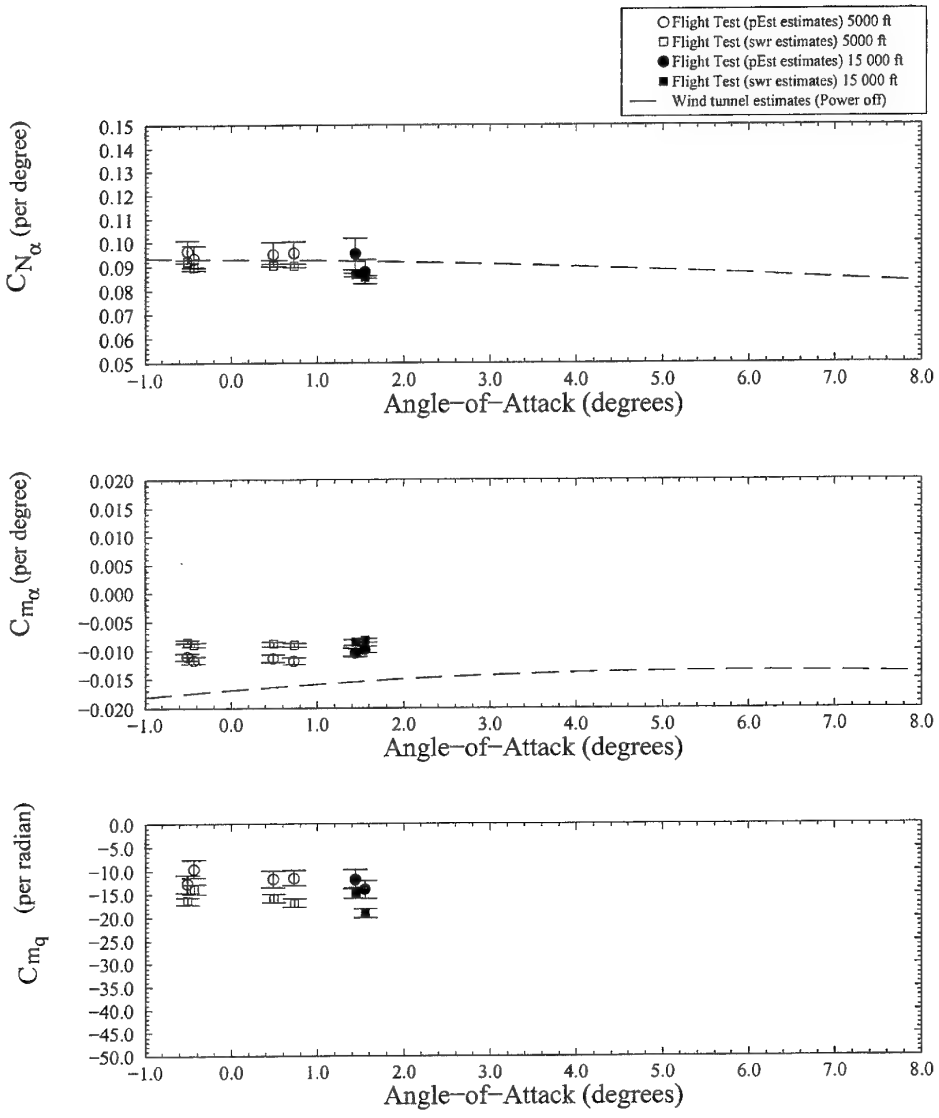

Figure 4: PC 9/A angle-of-attack and pitch rate derivatives, landing flap.

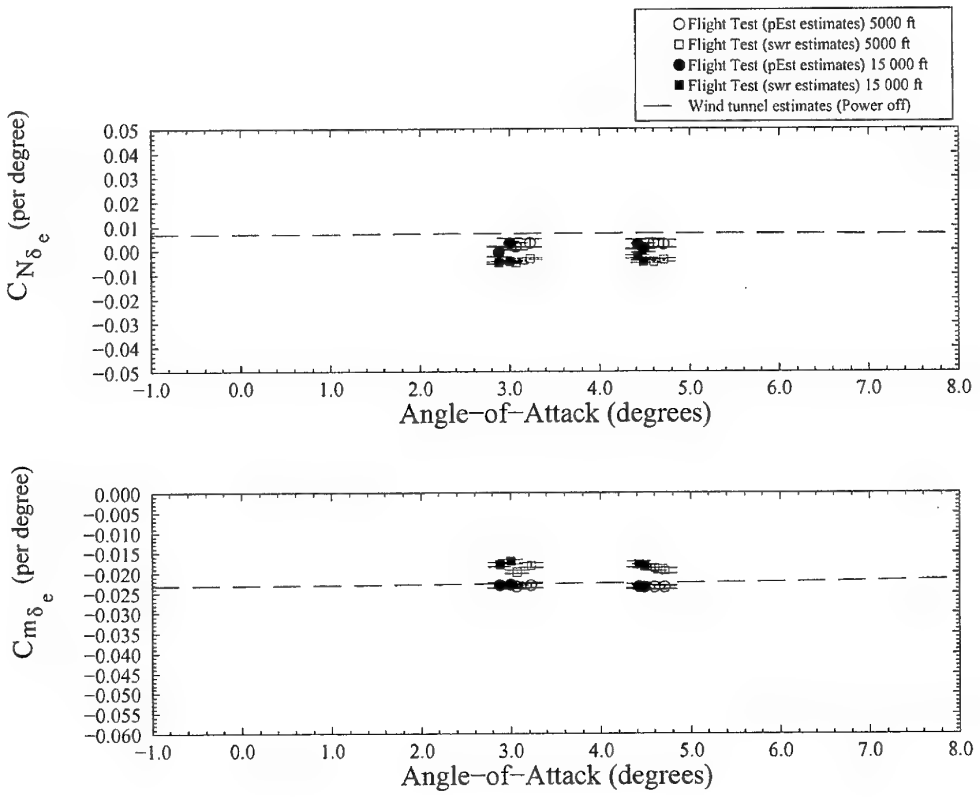

Figure 5: PC 9/A longitudinal control derivatives, gear down.

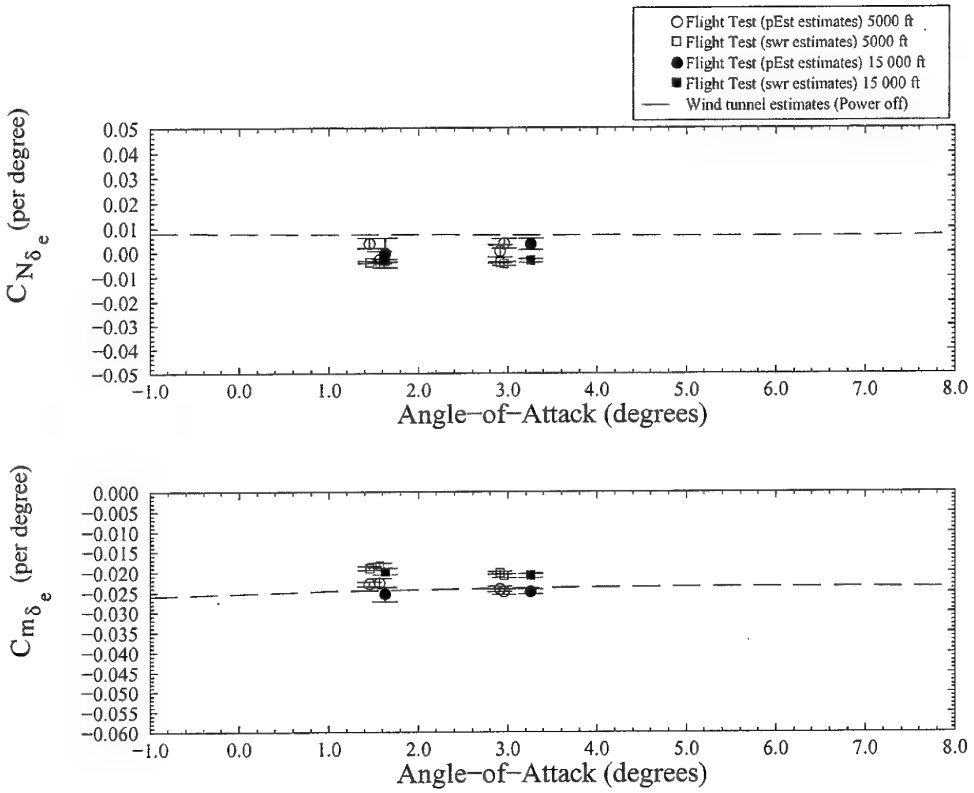

Figure 6: PC 9/A longitudinal control derivatives, take-off flap.

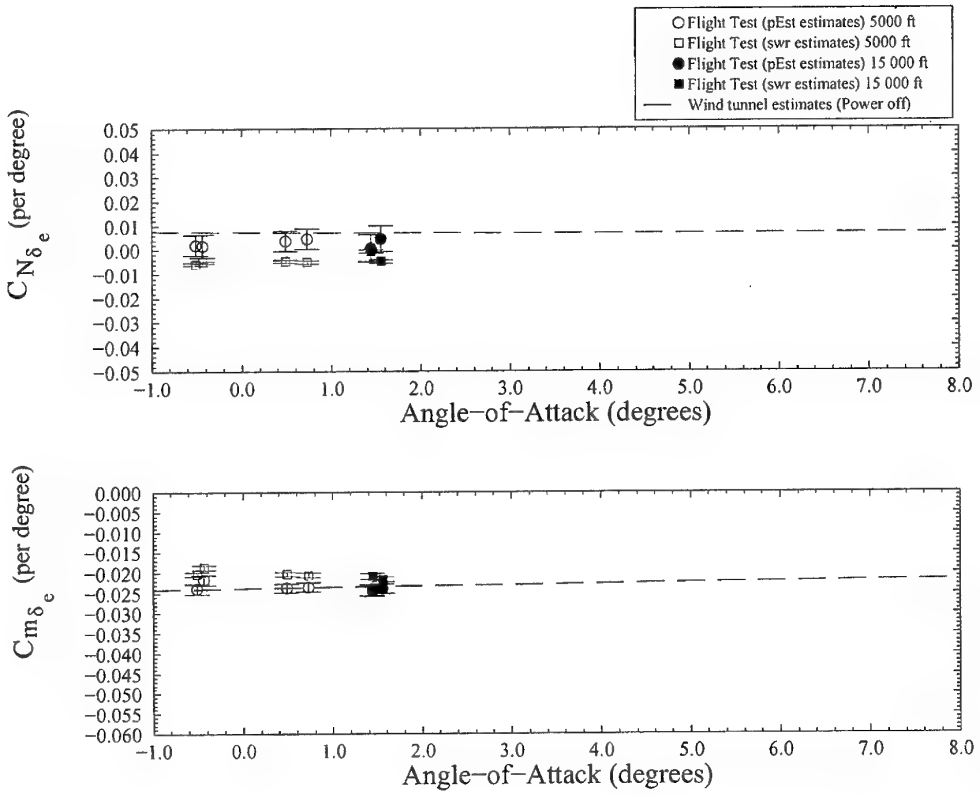

Figure 7: PC 9/A longitudinal control derivatives, landing flap.

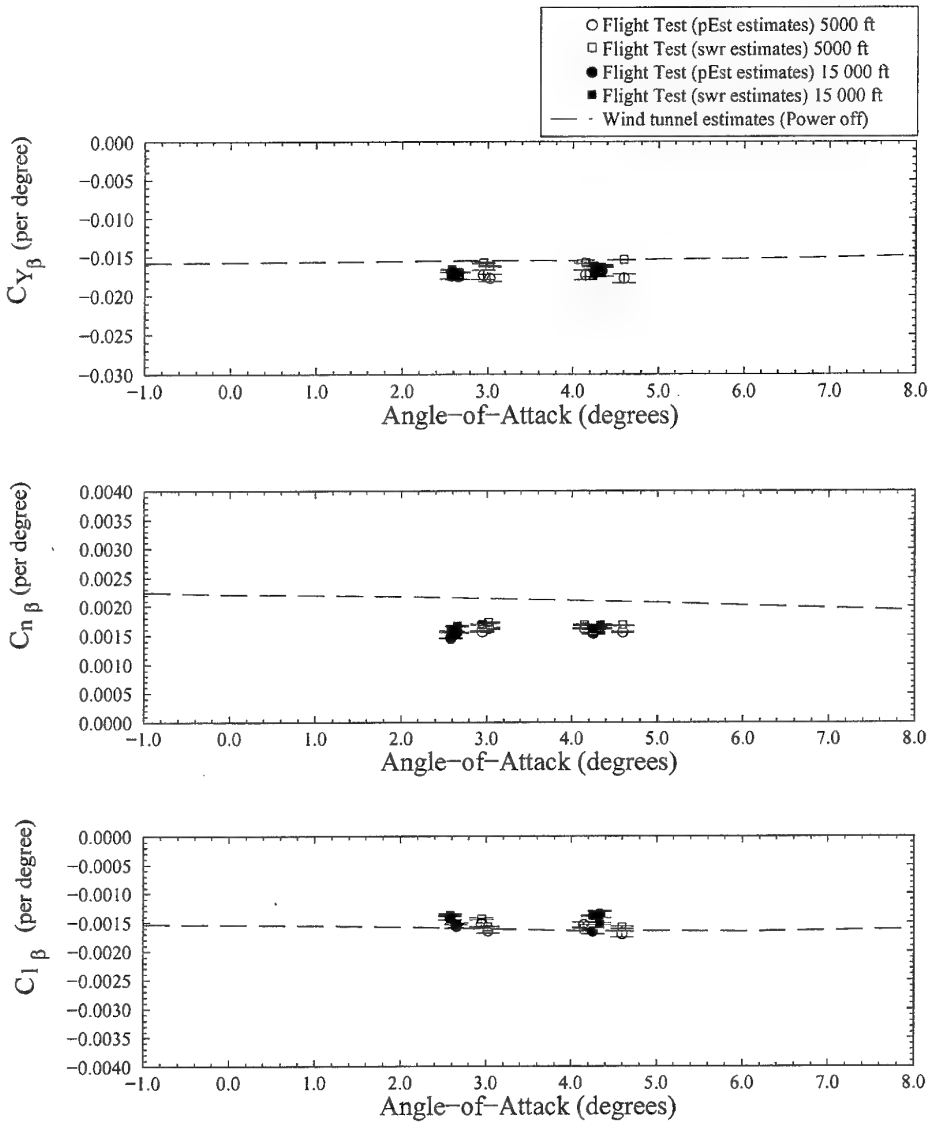

Figure 8: PC 9/A angle-of-sideslip derivatives, gear down.

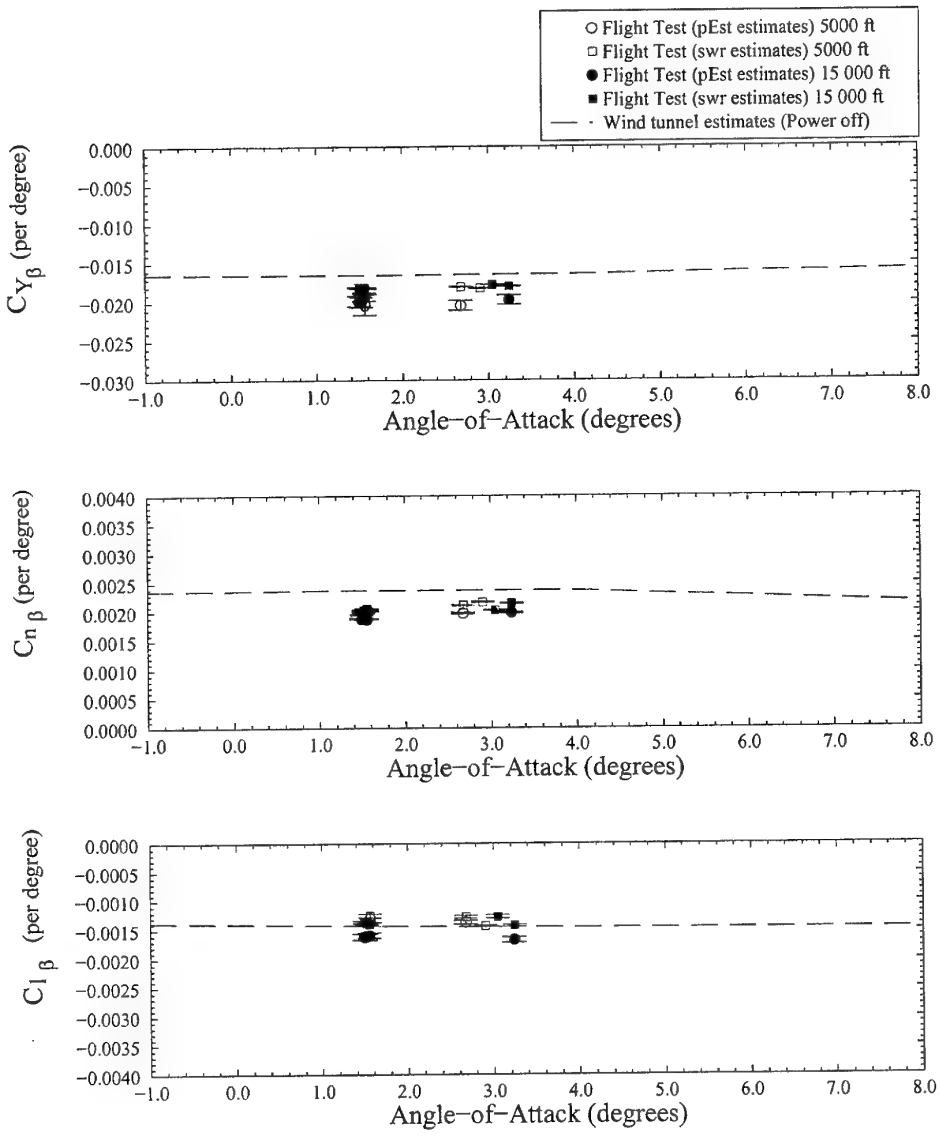

Figure 9: PC 9/A angle-of-sideslip derivatives, take-off flap.

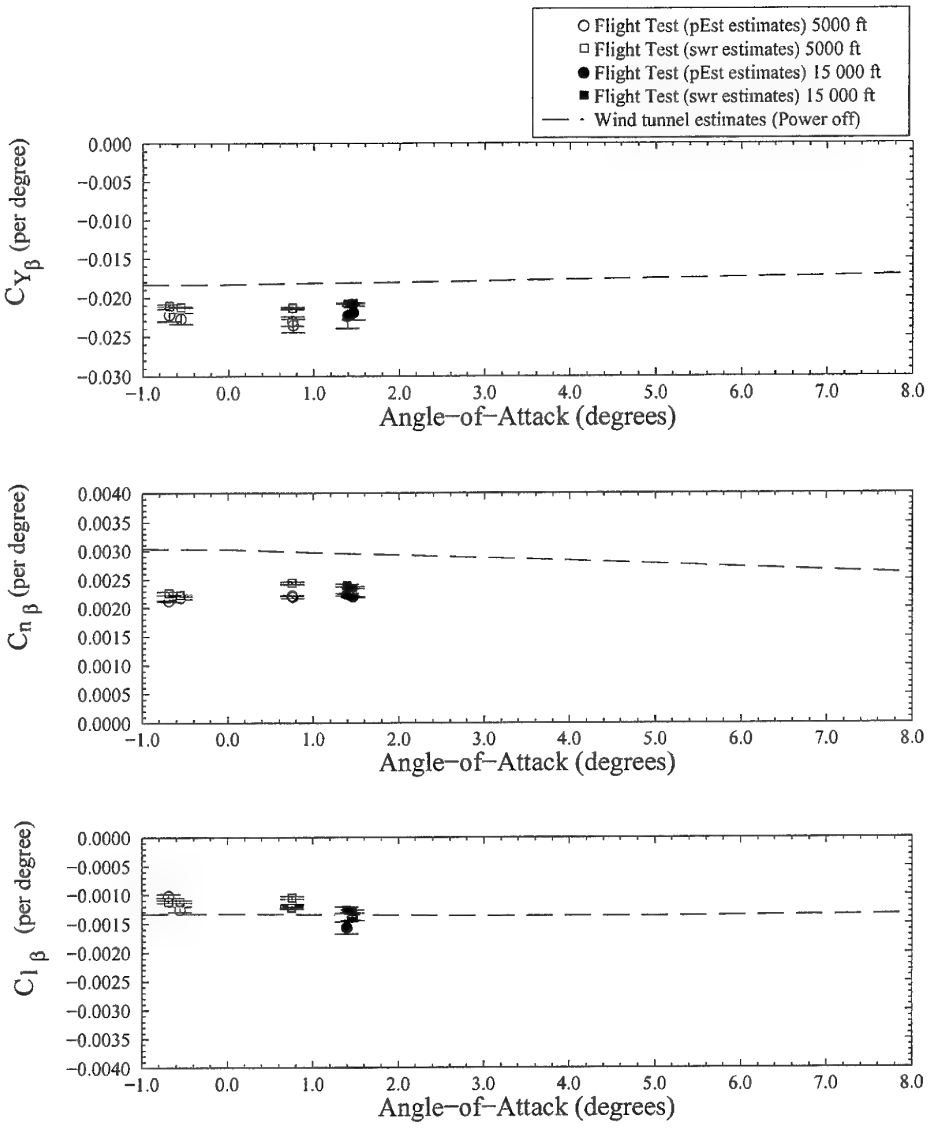

Figure 10: PC 9/A angle-of-sideslip derivatives, landing flap.

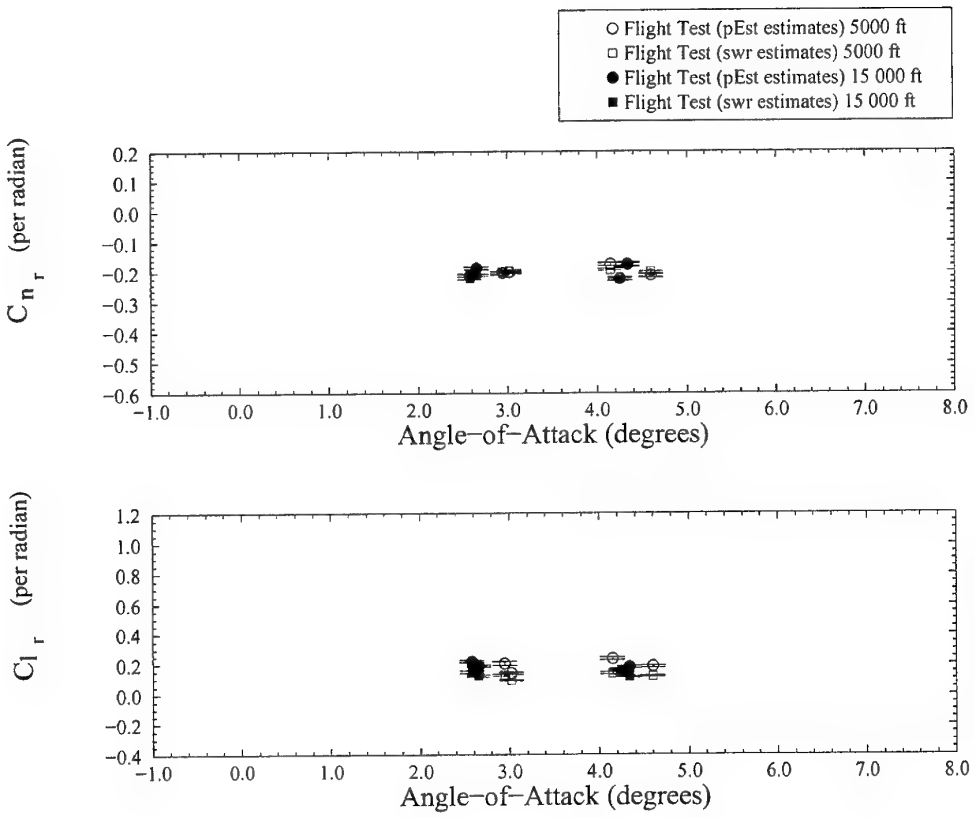

Figure 11: PC 9/A yaw rate derivatives, gear down.

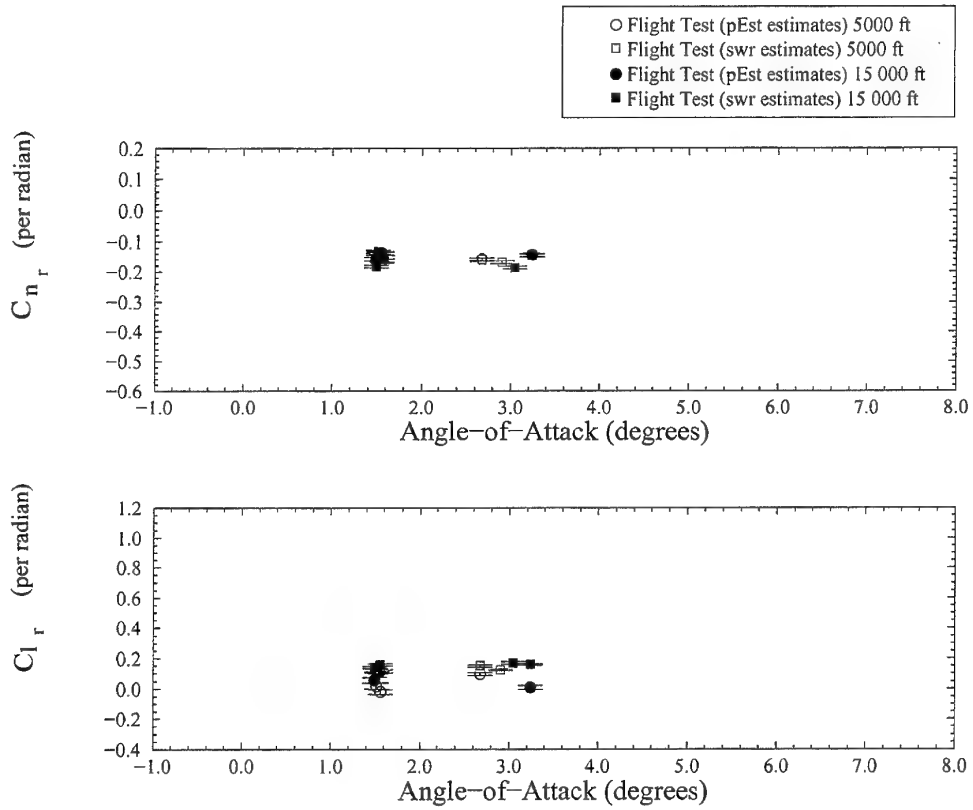

Figure 12: PC 9/A yaw rate derivatives, take-off flap.

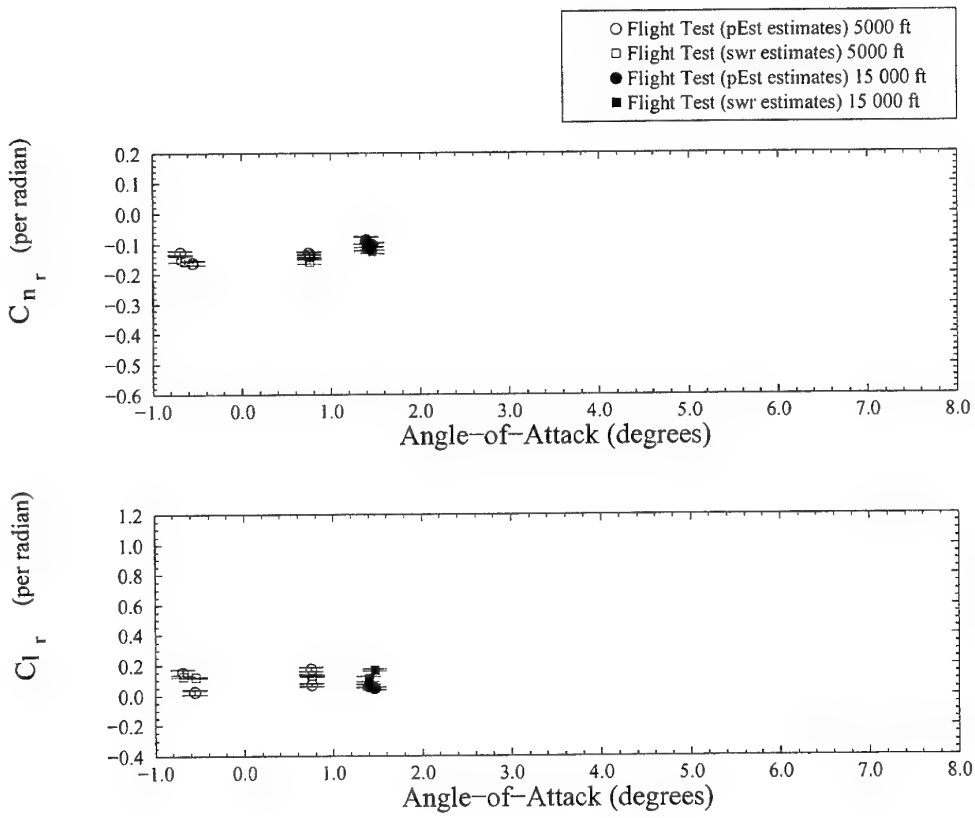

Figure 13: PC 9/A yaw rate derivatives, landing flap.

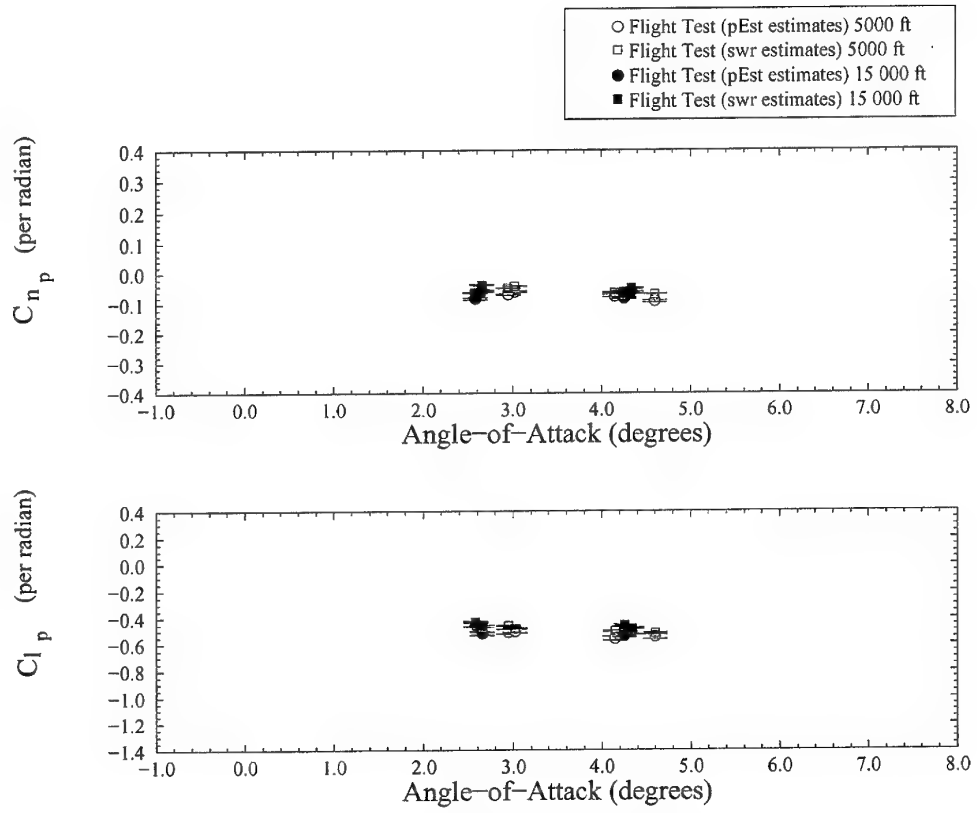

Figure 14: PC 9/A roll rate derivatives, gear down.

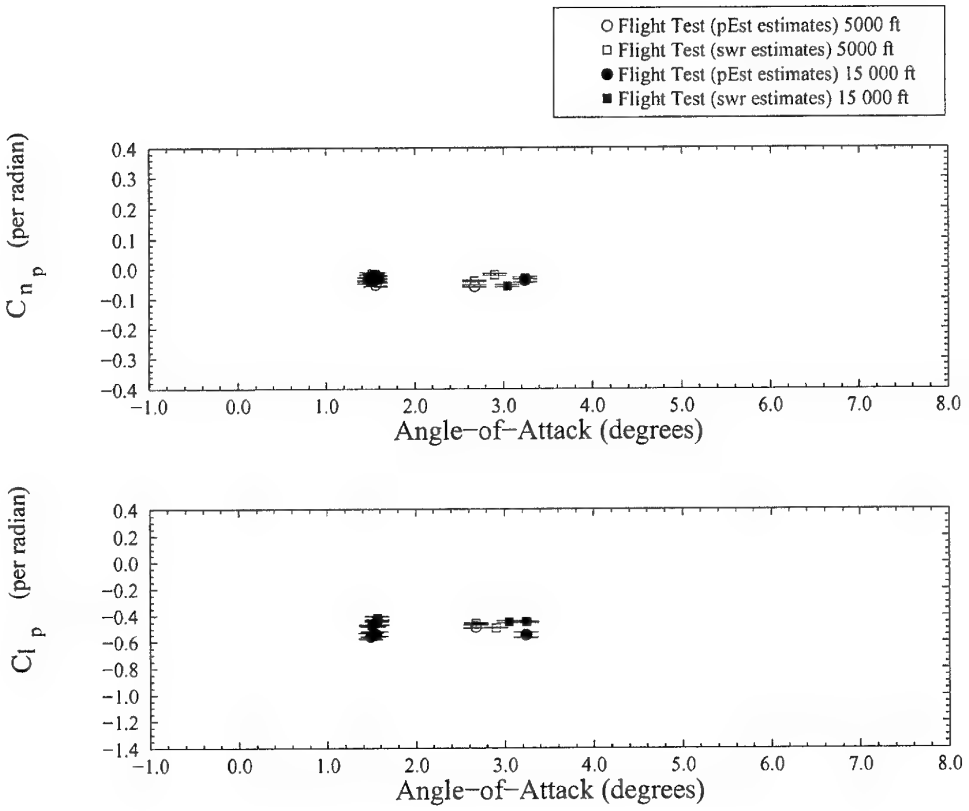

Figure 15: PC 9/A roll rate derivatives, take-off flap.

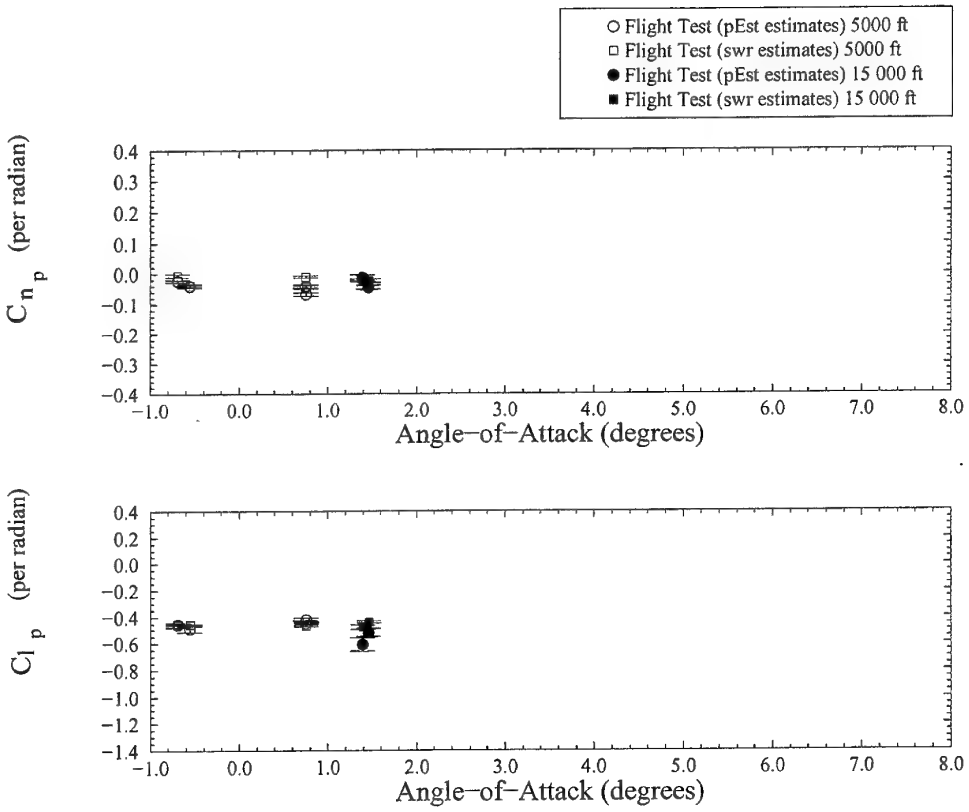

Figure 16: PC 9/A roll rate derivatives, landing flap.

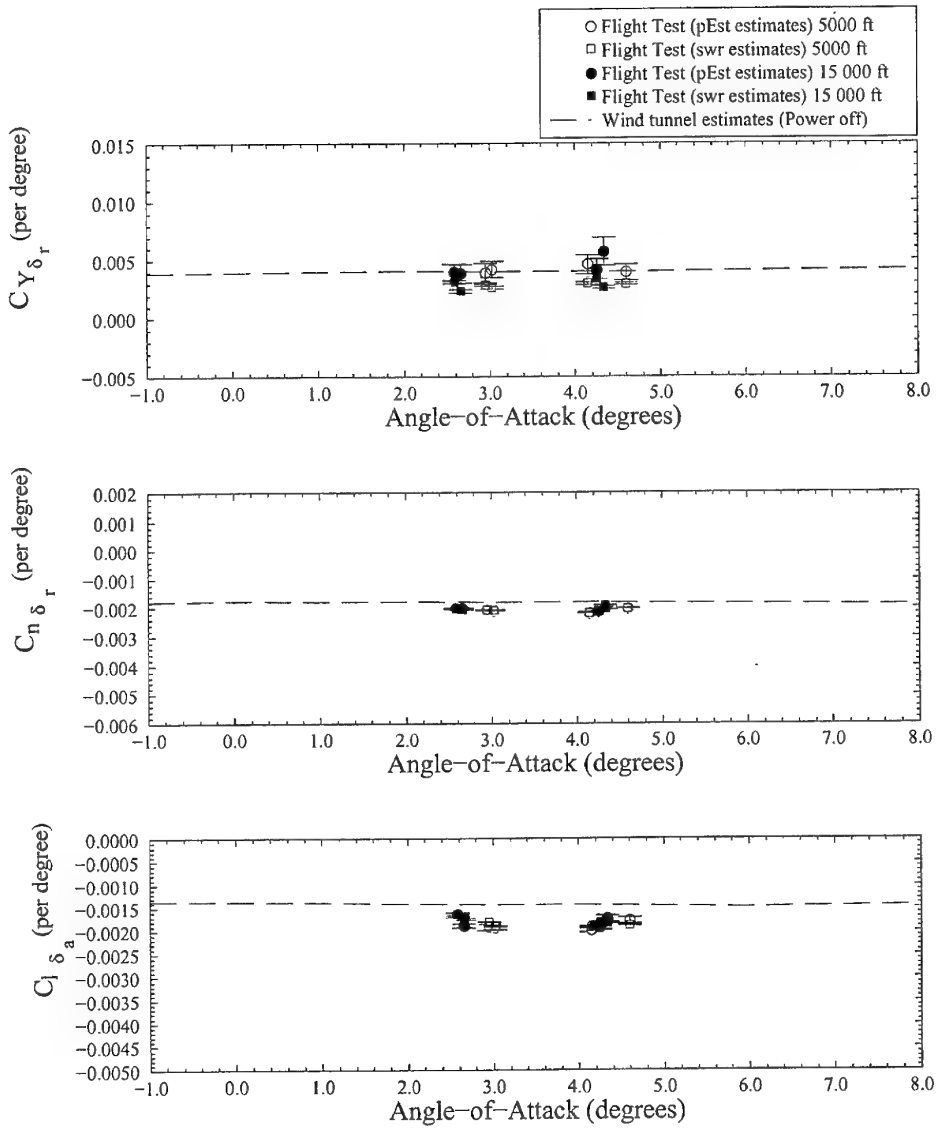

Figure 17: PC 9/A lateral control derivatives, gear down.

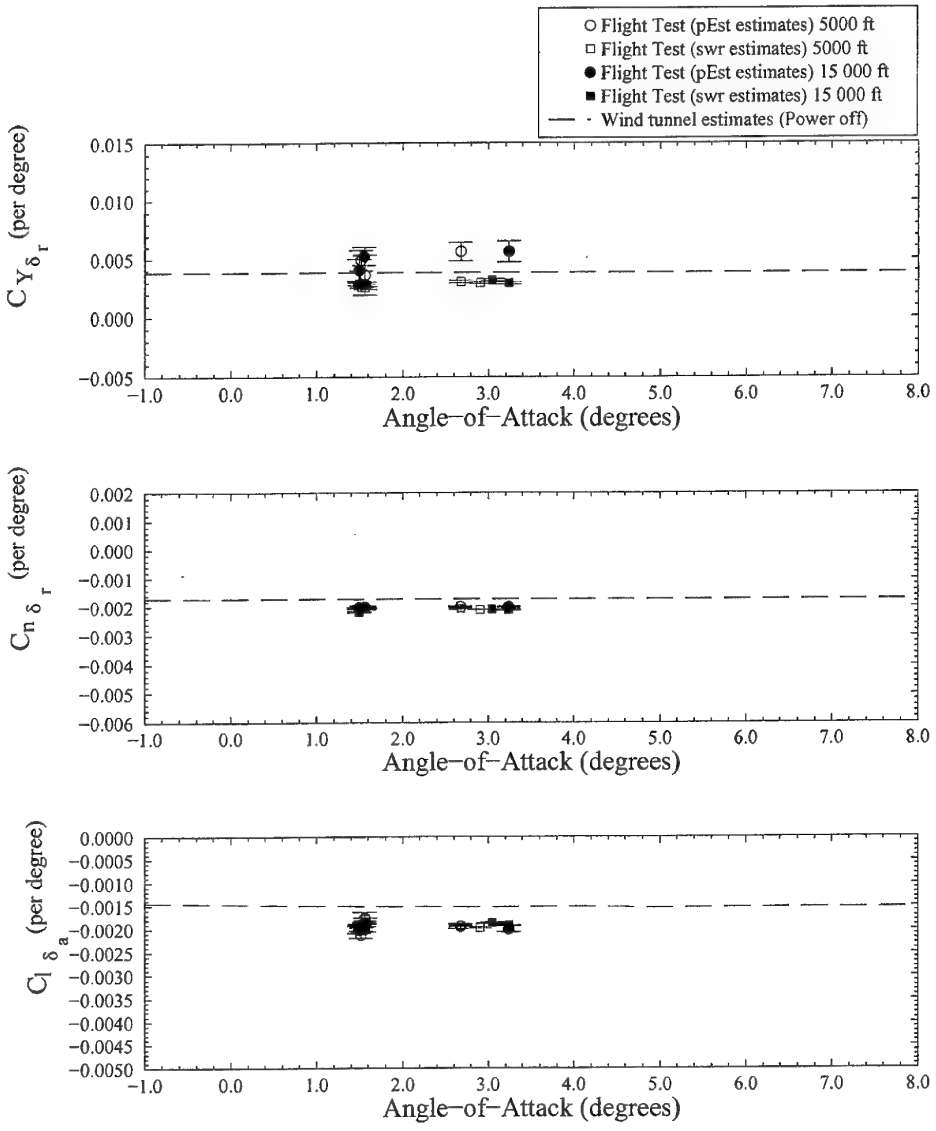

Figure 18: PC 9/A lateral control derivatives, take-off flap.

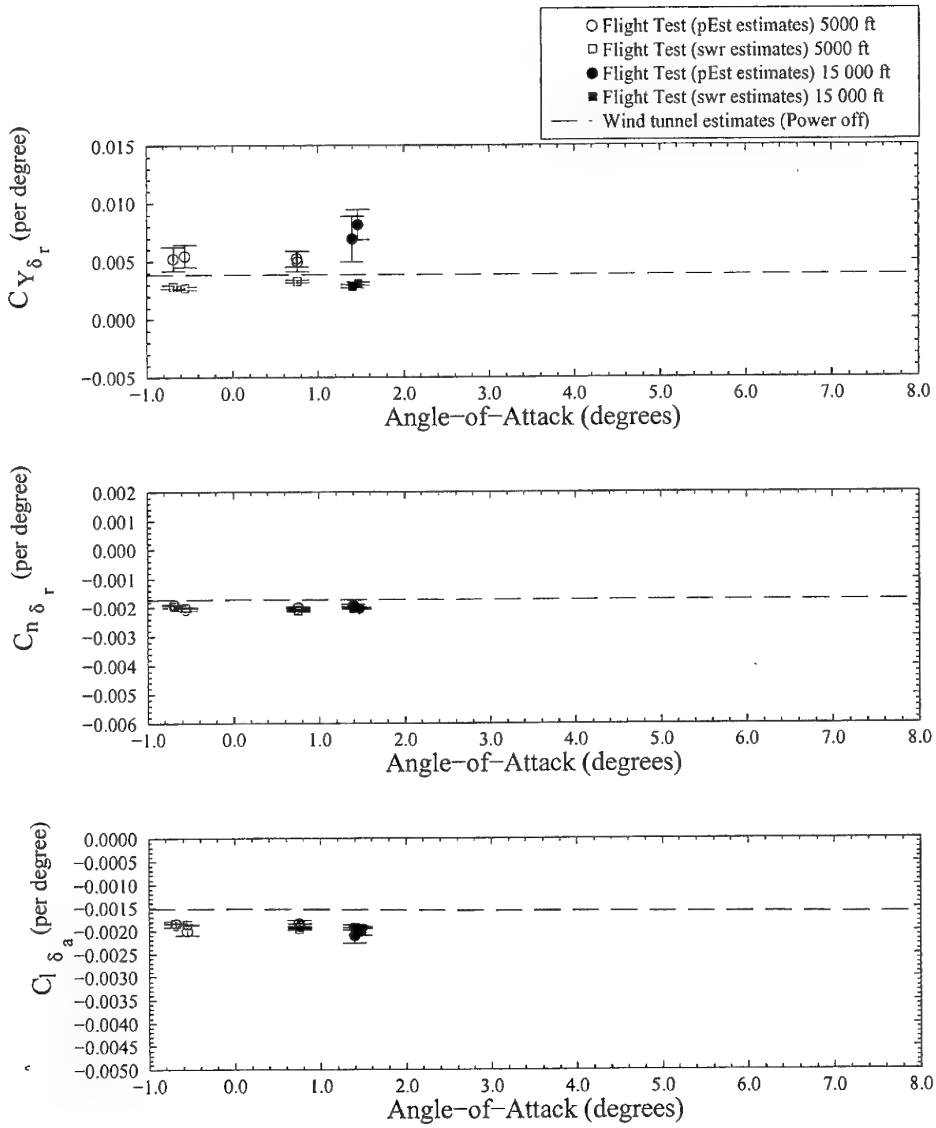

Figure 19: PC 9/A lateral control derivatives, landing flap.

Appendix A: Mass, Centre-of-Gravity and Mass Moments-of-Inertia

Equations for the mass, centre-of-gravity, and mass moments-of-inertia of the flight test article in clean configuration were derived as functions of fuel mass in reference [1, Appendix A]. These equations are summarised below.

$$M = 1866.1 + M_F \quad \text{(kg)} \tag{A1}$$

$$x_{c.g.} = \frac{8015.5+4.178M_F}{1866.1+M_F} \quad \text{(m)} \tag{A2}$$

$$I_{XX} = 2505.9 + 6.177\,(M - 1866.1) \quad \text{(kg.m}^2\text{)} \tag{A3}$$

$$I_{YY} = 6622.2 + 0.033\,(M - 1866.1) \quad \text{(kg.m}^2\text{)} \tag{A4}$$

$$I_{ZZ} = 8467.1 + 6.188\,(M - 1866.1) \quad \text{(kg.m}^2\text{)} \tag{A5}$$

$$I_{XY} = 49.0 + 0.0057\,(M - 1866.1) \quad \text{(kg.m}^2\text{)} \tag{A6}$$

$$I_{XZ} = 196.9 + 0.0041\,(M - 1866.1) \quad \text{(kg.m}^2\text{)} \tag{A7}$$

$$I_{YZ} = 3.0 + 0.0007\,(M - 1866.1) \quad \text{(kg.m}^2\text{)} \tag{A8}$$

During the flight test program, the clean aircraft longitudinal centre-of-gravity position varied between 4.27m (24.2%MAC) and 4.30m (25.6%MAC). The lateral and vertical centre-of-gravity positions were assumed to be invariant with fuel usage, and were fixed at values of 0.024m and -2.2m, respectively, relative to the aircraft datum.

For the purposes of analysing the approach and departure configuration flight test data, the above equations for centre-of-gravity location and mass moments-of-inertia have been

modified to account for the effects of deployment of the landing gear. The effect on centre-of-gravity location resulting from flap and speed brake deployment was assumed to be negligible.

Tables A1, A2, and A3 detail the clean aircraft basic mass distribution, retracted landing gear mass distribution, and deployed landing gear mass distribution, respectively. This data is sourced from references [3, 4, 18, 19]. All distances are relative to the aircraft datumn located 3 metres forward of the engine firewall and 2 metres below the forward fuselage reference line. The landing gear has been modelled as point masses located at the end of each leg.

	Mass (kg)	Moment Arm (m)
Basic Aircraft	1784.5	4.306
Pilot	81.6	4.061
Fuel	Variable	4.178

Table A1: Flight test aircraft mass distribution [3, 4].

	Mass (kg)	x (m)	y (m)	z (m)
Nose gear	42.0	3.45	0.00	1.90
Starboard main gear	45.3	4.62	0.50	1.90
Port main gear	45.3	4.62	-0.50	1.90

Table A2: Retracted landing gear mass and moment arm.

	Mass (kg)	x (m)	y (m)	z (m)
Nose gear	42.0	2.28	0.00	1.08
Starboard main gear	45.3	4.62	1.27	1.23
Port main gear	45.3	4.62	-1.27	1.23

Table A3: Deployed landing gear mass and moment arm.

The PC 9/A main gear deploys and retracts laterally with little or no longitudinal motion. Therefore, the effect of its deployment on the longitudinal centre-of-gravity location of the aircraft was assumed to be negligible. However, the effect of nose gear deployment on longitudinal centre-of-gravity location was taken into account. The longitudinal location of the aircraft centre-of-gravity, with landing gear deployed, is given by equation A9.

$$x_{c.g._{dep_{tot}}} = x_{c.g.} - \frac{m_{ng}}{m_{tot}} \left(x_{c.g._{ng_{ret}}} - x_{c.g._{ng_{dep}}} \right). \tag{A9}$$

Where m_{ng} is the mass of the nose gear, $x_{c.g._{ng_{ret}}}$ is the centre-of-gravity of the nose gear in the retracted position, $x_{c.g._{ng_{dep}}}$ is the centre-of-gravity of the nose gear in the deployed position, and $x_{c.g.}$ is the clean aircraft centre-of-gravity location. Substitution of the appropriate data into equation A9 yields,

$$x_{c.g._{dep_{tot}}} = x_{c.g.} - \frac{48.972}{m_{tot}}(\text{m}) \tag{A10}$$

This represents a forward longitudinal c.g. shift of approximately $0.5\%\bar{c}$.

Similar equations were developed to determine the change in the vertical c.g. position.

$$z_{c.g._{dep_{tot}}} = z_{c.g.} + \frac{m_{ng}}{m_{tot}}\left(z_{c.g._{ng_{dep}}} - z_{c.g._{ng_{ret}}}\right) + \frac{2m_{mg}}{m_{tot}}\left(z_{c.g._{mg_{dep}}} - z_{c.g._{mg_{ret}}}\right). \tag{A11}$$

As the vertical centre-of-gravity location of the clean aircraft was assumed constant, all terms except m_{tot}, in equation A11, were known. Substitution of the relevant data yields,

$$z_{c.g._{dep_{tot}}} = 2.200 - \frac{107.868}{m_{tot}}(\text{m}). \tag{A12}$$

This represents a vertical c.g. shift of approximately $2.2\%\bar{c}$ downwards.

To evaluate the effect of landing gear deployment on the mass moments-of-inertia of the aircraft, the data from tables A2 and A3 were used to evaluated the inertia of the individual gear components in both the retracted and deployed positions. The difference between the deployed values and the retracted values represents the increment that was added to the clean aircraft values yielding inertial data for the aircraft in approach and departure configurations. These increments are detailed in table A4.

Parameter	kg.m^2
ΔI_{XX}	249.70
ΔI_{YY}	266.70
ΔI_{ZZ}	263.80
ΔI_{XY}	1.16
ΔI_{XZ}	64.95
ΔI_{YZ}	2.70

Table A4: Mass moment-of-inertia increments due to landing gear deployment.

The inertia increments due to gear deployment were added to equations A3 to A8. This yielded the gear deployed inertia equations.

$$I_{XX_{dep_{tot}}} = 2505.9 + 6.177\,(M - 1866.1) \quad (\text{kg.m}^2) \tag{A13}$$

$$I_{YY_{dep_{tot}}} = 6622.2 + 0.033\,(M - 1866.1) \quad (\text{kg.m}^2) \tag{A14}$$

$$I_{ZZ_{dep_{tot}}} = 8467.1 + 6.188\,(M - 1866.1) \quad (\mathrm{kg.m^2}) \tag{A15}$$

$$I_{XY_{dep_{tot}}} = 49.0 + 0.0057\,(M - 1866.1) \quad (\mathrm{kg.m^2}) \tag{A16}$$

$$I_{XZ_{dep_{tot}}} = 196.9 + 0.0041\,(M - 1866.1) \quad (\mathrm{kg.m^2}) \tag{A17}$$

$$I_{YZ_{dep_{tot}}} = 3.0 + 0.0007\,(M - 1866.1) \quad (\mathrm{kg.m^2}) \tag{A18}$$

DISTRIBUTION LIST

A Correlation between Flight-determined Longitudinal and Lateral Derivatives and Wind Tunnel Data for the Pilatus PC 9/A Training Aircraft in Approach and Departure Configurations

Nick van Bronswijk, Andrew D. Snowden, Hilary A. Keating and Geoff J. Brian

	Number of Copies
DEFENCE ORGANISATION	
Task Sponsor	
CDR ARDU	1
S&T Program	
Chief Defence Scientist FAS Science Policy AS Science Corporate Management	1
Director General Science Policy Development	1
Counsellor, Defence Science, London	Doc Data Sht
Counsellor, Defence Science, Washington	Doc Data Sht
Scientific Adviser to MRDC Thailand	Doc Data Sht
Scientific Adviser Policy and Command	1
Navy Scientific Adviser	Doc Data Sht
Scientific Adviser, Army	Doc Data Sht
Air Force Scientific Adviser	1
Director Trials	1
Aeronautical and Maritime Research Laboratory	
Director, Aeronautical and Maritime Research Laboratory	1
Air Operations Division	
Chief, Air Operations Division	1
Research Leader, Avionics and Flight Mechanics	1
Head, Flight Mechanics Applications	1
Task Manager – G. J. Brian	1
Author – N. van Bronswijk	1
Author – A. D. Snowden	1
Author – H. A. Keating	1
J. S. Drobik	1
B. A. Woodyatt	1
K. L. Bramley	1
DSTO Libraries	
Library Fishermens Bend	Doc Data Sht

Library Maribyrnong	Doc Data Sht
Library Salisbury	1
Australian Archives	1
Library, MOD, Pyrmont	Doc Data Sht
US Defense Technical Information Center	2
UK Defence Research Information Centre	2
Canada Defence Scientific Information Service	1
NZ Defence Information Centre	1
National Library of Australia	1
Capability Systems Staff	
Director General Maritime Development	Doc Data Sht
Director General Land Development	Doc Data Sht
Director General C3I Development	Doc Data Sht
Director General Aerospace Development	1
Aircraft Research and Development Unit	
AERO1	1
Intelligence Program	
DGSTA Defence Intelligence Organisation	1
Manager, Information Centre, Defence Intelligence Organisation	1
Corporate Support Program (libraries)	
Officer in Charge, TRS, Defence Regional Library, Canberra	1
UNIVERSITIES AND COLLEGES	
Australian Defence Force Academy Library	1
Head of Aerospace and Mechanical Engineering, ADFA	1
Serials Section (M List), Deakin University Library, Geelong 3217	1
Senior Librarian, Hargrave Library, Monash University	1
Librarian, Flinders University	1
Head of Aeronautical Engineering, University of Sydney	1
Head of Centre of Expertise in Aerodynamic Loading, RMIT	1
OTHER ORGANISATIONS	
NASA (Canberra)	1
AusInfo	1

ABSTRACTING AND INFORMATION ORGANISATIONS

Library, Chemical Abstracts Reference Service	1
Engineering Societies Library, US	1
Materials Information, Cambridge Science Abstracts, US	1
Documents Librarian, The Center for Research Libraries, US	1

INFORMATION EXCHANGE AGREEMENT PARTNERS

Acquisitions Unit, Science Reference and Information Service, UK	1
Library – Exchange Desk, National Institute of Standards and Technology, US	1
National Aerospace Library, Japan	1
National Aerospace Library, Netherlands	1

SPARES

N. van Bronswijk	5

Total number of copies:	53

DEFENCE SCIENCE AND TECHNOLOGY ORGANISATION DOCUMENT CONTROL DATA				1. CAVEAT/PRIVACY MARKING
2. TITLE A Correlation between Flight-determined Longitudinal and Lateral Derivatives and Wind Tunnel Data for the Pilatus PC 9/A Training Aircraft in Approach and Departure Configurations			3. SECURITY CLASSIFICATION Document (U) Title (U) Abstract (U)	
4. AUTHORS Nick van Bronswijk, Andrew D. Snowden, Hilary A. Keating and Geoff J. Brian			5. CORPORATE AUTHOR Aeronautical and Maritime Research Laboratory 506 Lorimer St, Fishermans Bend, Victoria, Australia 3207	
6a. DSTO NUMBER DSTO–TR–0479	6b. AR NUMBER AR-011-629		6c. TYPE OF REPORT Technical Report	7. DOCUMENT DATE November, 2000
8. FILE NUMBER M1/9/760	9. TASK NUMBER AIR 00/205	10. SPONSOR CDR ARDU	11. No OF PAGES 40	12. No OF REFS 19
13. URL OF ELECTRONIC VERSION http://www.dsto.defence.gov.au/corporate/reports/DSTO–TR–0479.pdf			14. RELEASE AUTHORITY Chief, Air Operations Division	
15. SECONDARY RELEASE STATEMENT OF THIS DOCUMENT *Approved For Public Release* OVERSEAS ENQUIRIES OUTSIDE STATED LIMITATIONS SHOULD BE REFERRED THROUGH DOCUMENT EXCHANGE, PO BOX 1500, SALISBURY, SOUTH AUSTRALIA 5108				
16. DELIBERATE ANNOUNCEMENT No Limitations				
17. CITATION IN OTHER DOCUMENTS No Limitations				
18. DEFTEST DESCRIPTORS Flight tests Landing Lateral stability Longitudinal stability			PC 9/A aircraft System identification Take-off Wind tunnel tests	
19. ABSTRACT A series of flight tests were conducted on the PC 9/A aircraft, A23-045, at the Royal Australian Air Force's Aircraft Research and Development Unit. System identification techniques were applied to the data obtained from these flight tests to determine the stability and control derivatives of the aircraft. The longitudinal and lateral results for the aircraft in approach and departure configurations are presented in this report and comparisons are made with wind tunnel estimates.				